Toxoplasma gondii Coq1 is a heptaprenyl diphosphate synthase and its inhibition by a lipophilic bisphosphonate protects mice against *T. gondii* infection

Melissa A. Sleda[#1,2], Zhu-Hong Li[#1], Ranjan Behera[1], Baihetiya Baierna[1,2], Catherine Li[1], Jomkwan Jumpathong[3], Satish R. Malwal[4], Makoto Kawamukai[3], Eric Oldfield[4] and Silvia N. J. Moreno*[1,2]

[1]Center for Tropical and Emerging Global Diseases, University of Georgia, Athens, GA, USA
[2]Department of Cellular Biology, University of Georgia, Athens, GA, USA
[3]Department of Life Sciences, Life and Environmental Sciences and Institute of Agricultural and Life Sciences, Shimane University, Matsue, 690-8504, Japan
[4]Department of Chemistry, University of Illinois at Urbana Champaign, Urbana, IL, USA

*To whom correspondence should be addressed: Center for Tropical and Emerging Global Diseases and Department of Cellular Biology, University of Georgia, 350A Paul D. Coverdell Center, 500 D.W. Brooks Dr., Athens, GA 30602, Tel: 706-542-4736; Fax: 706-542-9493; Email: smoreno@uga.edu

#Equal contribution

Running title: TgCoq1 as a drug target

Key words: *Toxoplasma gondii*, isoprenoids, ubiquinone, mitochondria, bisphosphonate

Abstract

Prenyldiphosphate synthases catalyze the reaction of allylic diphosphates with one or more isopentenyl diphosphate molecules to form compounds such as farnesyl diphosphate, used in e.g. sterol biosynthesis and protein prenylation, as well as longer "polyprenyl" diphosphates, used in ubiquinone and menaquinone biosynthesis. Quinones play an essential role in electron transport and are associated with the inner mitochondrial membrane due to the presence of the polyprenyl group. In this work, we investigated the synthesis of the polyprenyl diphosphate that alkylates the ubiquinone ring precursor in *Toxoplasma gondii*, an opportunistic pathogen that causes serious disease in immunocompromised patients and the unborn fetus. The enzyme that catalyzes this early step of the ubiquinone synthesis is Coq1 (TgCoq1), and we show that it produces the C35 species, heptaprenyl diphosphate. TgCoq1 localizes to the mitochondrion, and is essential for *in vitro T. gondii* growth. We demonstrate that the growth defect of a *T. gondii* TgCoq1 mutant is rescued by complementation with a homologous *TgCoq1* gene or with a (C45) solanesyl diphosphate synthase from *Trypanosoma cruzi* (TcSPPS). We find that a lipophilic bisphosphonate (BPH-1218) inhibits *T. gondii* growth at low nM concentrations, while overexpression of the TgCoq1 enzyme dramatically reduced growth inhibition by the bisphosphonate. Both the severe growth defect of the mutant and the inhibition by BPH-1218 were rescued by supplementation with a long chain (C30) ubiquinone (UQ_6). Importantly, BPH-1218 also protected mice against a lethal *T. gondii* infection. TgCoq1 thus represents a potential drug target that could be exploited for improved chemotherapy of toxoplasmosis.

Importance

Millions of people are infected with *Toxoplasma gondii* and the available treatment for toxoplasmosis is not ideal. Most of the drugs currently used are only effective for the acute infection and treatment can trigger serious side-effects requiring changes in the therapeutic approach. There is, therefore, a compelling need for safe and effective treatments for toxoplasmosis. In this work, we characterize an enzyme of the mitochondrion of *T. gondii* that can be inhibited by an isoprenoid pathway inhibitor. We present several evidences that demonstrate that inhibition of the enzyme is linked to parasite death. In addition, the drug is able to protect mice against a lethal dose of *T. gondii*. Our results thus reveal a promising chemotherapeutic target for the development of new medicines for toxoplasmosis.

33 **Introduction**

34 Apicomplexan parasites are responsible for important human and animal diseases including
35 malaria and toxoplasmosis. The phylum member *Toxoplasma gondii* alone causes toxoplasmosis
36 in aproximately one-third of the world's population (1). Most human infections are uncomplicated,
37 but severe disease and death can occur in prenatal infections and in immunocompromised
38 individuals (2). In the United States there is an estimated 11% seroprevalence, with ~1.1 million
39 people infected each year with *T. gondii* (3). Treatment for toxoplasmosis is challenged by the lack
40 of an effective treatment for the chronic infection, and many patients do not respond to therapy
41 (4). Most of the drugs currently used are poorly distributed to the central nervous system and they
42 can trigger serious side-effects requiring changes in the therapeutic approach (5). There is,
43 therefore, a compelling need for safe and effective treatments for toxoplasmosis.

44 The mitochondrion of *T. gondii* is essential for its survival and is a validated drug target as it
45 houses important pathways like the Electron Transport Chain (ETC). Ubiquinone is an essential
46 component of the ETC, and it is confined to the inner mitochondrial membrane by a long
47 isoprenoid tail (6). Ubiquinone biosynthesis in *T. gondii* is a relatively unexplored subject, but
48 what it is known is that isoprenoid biosynthesis is essential for cell growth (7). Isoprenoids are
49 lipid compounds found in nature and they have many important functions (8, 9). The enzymes that
50 synthesize and use isoprenoids are among the most important drug targets for the treatment of
51 cardiovascular disease, osteoporosis and bone metastases and have shown promise as
52 antimicrobials (10-12). The five carbon (C5) precursors of isoprenoids, isopentenyl diphosphate
53 (IPP) and dimethylallyl diphosphate (DMAPP) (Fig. 1A) (13) are synthesized in mammalian cells
54 by the mevalonate pathway, while other organisms—including apicomplexan parasites—use the
55 1-deoxy-D-xylulose-5-phosphate (DOXP) pathway (7)(Fig. 1A, green square). The enzyme
56 farnesyl diphosphate synthase (FPPS) synthesizes farnesyl diphosphate (FPP) from DMAPP and
57 IPP and further elongation of FPP results in (C20) geranylgeranyl diphosphate (GGPP), a reaction
58 catalyzed by GGPP synthases (GGPPS). Notably, *T. gondii* expresses a FPPS (TgFPPS) that
59 synthesizes both FPP and GGPP (14). We also previously showed that intracellular parasites are
60 capable of acquiring GGPP from the host (15), making parasites resistant to bisphosphonate
61 inhibitors of the *T. gondii* FPPS, such as zoledronate, but also sensitive to inhibition of the
62 mammalian isoprenoid biosynthesis pathway (15). It thus appeared possible that inhibiting the
63 prenyldiphosphate synthase responsible for biosynthesis of the longer-chain species involved in
64 ubiquinone biosynthesis might be an alternate therapeutic strategy.

65 In this work we characterize the enzyme (*TgCoq1*) responsible for the synthesis of the
66 isoprenoid chain that supplies the tail of the mitochondrial ubiquinone, as well as determine its
67 biological function in the parasites. In addition, we show that specific inhibition of TgCoq1
68 impacts parasite growth, as well as its virulence in mice. Our results thus reveal that TgCoq1 is a
69 promising chemotherapeutic target for the development of new medicines for toxoplasmosis.
70

71 **RESULTS**

72

73 **Identification of *T. gondii* Coq1**. The *T. gondii* gene *TGGT1_269430* annotated in ToxoDB as a
74 polyprenyl synthase predicts the expression of a protein of 676 amino acids with a calculated
75 molecular mass of 72.5 kDa and an isoelectric point of 8.54. The deduced *T. gondii* polypeptide
76 sequence was aligned with other representative polyprenyl diphosphate synthases (Fig. S1) to
77 highlight the specific domains, in particular the first aspartic rich motif (FARM) and the second
78 aspartic rich motif (SARM) involved in substrate recognition (14); the chain-length-determining
79 (CLD) region, as well as a long N-terminal sequence thought to be involved in mitochondrial
80 targeting. All the conserved motifs involved in catalysis or binding (regions I–VII) identified in
81 other polyprenyl synthases (16) are present in the *T. gondii* enzyme (Fig. S1). The presence of
82 small residues (Ser and Ala) at positions 4 and 5 prior to the first aspartate-rich motif (FARM)
83 predicts that the active site of the enzyme will accommodate long-chain isoprenoid products (17).
84 These residues are Phe in human FPPS, which makes only the C15 compound FPP. That is, bulky
85 amino acids would not permit the nascent isoprenoid chains to extend further inside the
86 hydrophobic cavity of the enzyme. A BLAST search of the protein data base showed that the
87 amino acid sequence from *T. gondii* shared 81.31% identity with *Neospora caninum*, another
88 apicomplexan polyprenyl diphosphate synthase. For the human homologue (accession number
89 NP_055132), the identity was 31.15% (18). We named this gene *TgCoq1*, following the
90 established nomenclature of ubiquinone biosynthesis enzymes (6).
91 A phylogenetic comparison of the TgCoq1 sequence with representative animal, plant, yeast
92 and other apicomplexan long prenyl diphosphate synthases (Fig. 1B and Table S1) showed that
93 TgCoq1 groups with long-chain isoprenoid-biosynthesis enzymes from other organisms and is
94 most closely related to other apicomplexan enzymes known or predicted to be involved in the
95 synthesis of long-chain prenyldiphosphates. Notably, the *T. gondii* Coq1 protein is predicted to

96 have a very long N-terminal domain, which was not reported in earlier annotations of ToxoDB.
97 We used multiple programs to analyze the mitochondrial targeting sequence prediction and
98 cleavage site. TargetP 2.0 program predicts 0.94 and MitoProt II predicts 0.7689 probability of
99 targeting to mitochondria. The MitoProt II program also predicts the presence of a cleavage site
100 54 aa from the N terminal. A similar N-terminal extension is found in the orthologous gene of
101 *Hammondia hammondi*, an avirulent relative of *T. gondii,* but has not yet been reported in other
102 apicomplexan sequences.

103 To delve more into the structure of TgCoq1 we next used the Phyre2 program (19) for structure
104 prediction. Using a diverse range of templates, several similar structures were predicted with 100%
105 confidence (with an average of ~30% identity). However, in all cases, only approximately one-
106 half of the protein structure—the catalytic C-terminal domain— was successfully predicted, as
107 shown in Figure 1C. The predicted structure of the catalytic domain of the *H. hammondi* protein
108 is quite similar and it is shown in Figure 1D.

109 Of note, a long N-terminal domain is also found in the previously characterized *T. gondii* FPPS
110 (TgFPPS) (14), a protein with 646 residues, slightly smaller than TgCoq1 (676 residues). The
111 Phyre2 structure prediction for TgFPPS is shown in Figure 1E and again, only the catalytic domain
112 can be successfully predicted. Figure 1F shows a superposition of the predicted structures for
113 TgCoq1 (green) and the TgFPPS (cyan) showing high similarity. Figure 1G shows a zoomed-in
114 view of Figure 1F (same color scheme) with the Ser/Ala/Phe CLD region indicated. From these
115 results and >100 previously reported FPPS structures, we concluded that the presence of the bulky
116 residues FF at positions 4 and 5 upstream to the SARM are found exclusively in the enzymes that
117 synthesize the C15 isoprenoid product (e.g. human FPPS), while the aminoacids CF are present in
118 the bifunctional TgFPPS, which synthesizes C15 as well as C20. For the polyprenyl synthase,
119 TgCoq1, the aminoacids at the same position are AS, enabling extensive chain elongation.
120 However, the H-bond network seen in the neutron crystallographic structure of human FPPS and
121 proposed to be involved in H^+ transport in all *trans*-head-to-head prenylsynthases (20, 21) is also
122 present in TgCoq1. Specifically for the HsFPPS/TgCoq1 comparison: Thr-201/Thr-499; Gln-
123 240/Gln-536; Asp-243/Asp-539; Asp-244/Asp-540; Tyr-193/Tyr-491 are predicted to have similar
124 interactions, as it is found in longer-chain species, such as hexaprenyl and heptaprenyl diphosphate
125 synthases (22, 23).

126 We next considered possible 'physical' properties of the N-terminal regions in TgCoq1, as
127 well as TgFPPS. We used the HeliQuest program (24) to investigate the hydrophobicity <**H**>,

128 hydrophobic moment <**μH**) and charge in the N-terminal regions of both proteins (Figs. S2A, S2B
129 and Table S2). The N-terminus of TgCoq1 appears to have a hydrophobic region (closest to the
130 actual N-terminus), followed by a very polar cationic domain, and then an anionic domain. In sharp
131 contrast, no such pattern was observed in the N-terminus of the TgFPPS (Fig. S2B), suggesting
132 the possibility that the N-termini might have different targets. We show in Table S2 helical wheel
133 representations of the 3 regions using an 18 residue α-helix scan in which the likely
134 neutral/hydrophobic, cationic and then anionic regions, with net charges of 0, +5 and -5, are shown.
135 These regions are not apparent in the sequence of the TgFPPS, which instead is highly enriched in
136 serine residues (14). There is only a ~10 residues sheet secondary structure predicted, all other
137 residues being either in helical or disordered regions.
138 In summary, the structures of the catalytic domains of TgCoq1 and TgFPPS are predicted to
139 be very similar. However, both proteins have extended N-terminal domains, and with the exeption
140 of the polyprenyl synthase sequence of *Hammondia hammondi*, they are not found in any other
141 polyprenyl synthase sequence. As discussed below, these domains are important for mitochondrial
142 targeting and perhaps, for other functions that remain to be determined.
143
144 **TgCoq1 synthesizes heptaprenyl diphosphate and *T. gondii* produces ubiquinone 7 (UQ_7)**
145 To investigate the biochemical function of TgCoq1 we cloned the *TGGT1_269430* gene in an *E.*
146 *coli* expression plasmid which also includes an N-terminal polyhistidine tag to facilitate the
147 purification of the recombinant protein by affinity chromatography. The activity of the purified
148 protein was measured with allylic substrates and co-substrates, by measuring the amount of IPPs
149 incorporated into the different long chain polyprenols (FPP and GGPP) (Fig. 2A). The reaction
150 product was dephosphorylated and analyzed by reverse-phase thin layer chromatography (TLC),
151 which showed labeling of a C35 product (Fig. 2B), indicating that TgCoq1 synthesizes heptaprenyl
152 diphosphate. A parallel experiment with the already characterized recombinant *Trypanosoma cruzi*
153 solanesyl diphosphate synthase (25), TcSPPS, known to synthesize a 45-carbon product, is shown
154 in the same TLC (Fig. 2B). Using a standard enzymatic method (25), the activity of TgCoq1 was
155 shown to be more efficient with FPP than with GGPP (Fig. 2C) or GPP as substrate (Table 1). The
156 kinetic parameters of the reaction using different substrates is shown in Table 1.
157 Since the length of the isoprenoid unit synthesized by Coq1 defines the type of UQ found in
158 cells, we next extracted freshly purified tachyzoites and analyzed the extracts by TLC followed by

159 HPLC and mass spectrometry (Fig. 2D). Standards for UQ_6, UQ_7, UQ_8, UQ_9, and UQ_{10} were run
160 and the retention time for the ubiquinone isolated from *T. gondii* coincides with that of UQ_7. The
161 MS spectra shown in Fig. 2D highlights the specific m/z value of UQ_7 in the form of ammonium
162 adduction. The amount of UQ_7 was quantified and found to be 4.2 μg/10^{10} tachyzoites (Fig. S3A).
163 We further validated the heptaprenyl diphosphate synthesis activity of TgCoq1 by expressing
164 the gene in *E. coli* and extracting UQ (Fig. S3B and C). As shown in Fig. S3C, the synthesis of
165 UQ_7 is enhanced after bacteria was induced to express TgCoq1, indicating TgCoq1 is functional
166 in *E. coli* without requiring another subunit while the fission yeast and the human decaprenyl
167 diphosphate synthase enzymes required two subunits for functionality (18, 26).
168 In summary, TgCoq1 synthesizes heptaprenyl diphosphate, a C35 species, and *T. gondii* makes
169 UQ_7, supporting the role of TgCoq1 as heptaprenyl diphosphate synthase.
170

171 **TgCoq1 is essential for *T. gondii* growth and localizes to the mitochondria**

172 To investigate the subcellular localization of TgCoq1 we introduced a triple HA (human
173 influenza hemagglutinin) epitope-tag at the 3' end of the *TgCoq1* gene locus and isolated *TgCoq1-*
174 *HA* clones resistant to chloramphenicol (Fig. 3A). We found that TgCoq1 co-localizes with the
175 mitochondrial marker MitoTracker (Fig. 3B). We next modified the 5' region of the *TgCoq1-HA*
176 mutant inserting a tetracycline (ATc)-regulatable element (27) and isolated the *i*Δ*Coq1-HA* mutant
177 in which the expression of the tagged TgCoq1 is controlled with anhydrotetracycline, ATc (Fig.
178 3A). The parental cell line was the *TatiΔku80* which combines regulated gene expression (27) with
179 higher efficiency of homologous recombination (28). We complemented the *i*Δ*Coq1-HA* mutant
180 with the *TgCoq1* cDNA (*i*Δ*Coq1-coq1*) or with a cosmid (PSBME30) (*i*Δ*Coq1-cosmid*) containing
181 the *TgCoq1* genomic locus. These genetic modifications generated the mutants *i*Δ*Coq1-HA,*
182 *i*Δ*Coq1-coq1* and *i*Δ*Coq1-cosmid* which were validated by Southern blot analysis (Fig. S4A).
183 Immunofluorescence analysis (IFA) showed that TgCoq1-3HA was not expressed after 3 days of
184 culture with ATc (Fig. 3B, *bottom row*). Western blots showed that the expression of TgCoq1 was
185 completely ablated at day 3 with ATc and significantly reduced at day 2 (Fig. 3C). We next
186 assessed growth of the mutant using plaque assays in which the parasite engages in repetitive
187 cycles of invasion, replication, and egress, lysing the host monolayer and forming plaques that can
188 be visualized by staining cultures with crystal violet. Preincubation of the mutant with ATc for 3
189 days prevented the formation of plaques in the *i*Δ*Coq1* cell line and this growth defect was restored

190 in the complemented *iΔCoq1-coq1* mutant (Fig. 3D-E). To further characterize the growth defect
191 of the *iΔCoq1* mutant we expressed a cytosolic fluorescent protein (tdTomato) in parental and
192 mutant (*iΔCoq1*) lines and used its fluorescence as a proxy for growth of clonal lines (29) (Fig.
193 3F). The growth defect of the *iΔCoq1* mutant was partially rescued by expression of Coq1 in the
194 *iΔCoq1-coq1* mutant (Fig. 3F). To further characterize the growth defect, we tallied the number of
195 parasites per parasitophorous vacuole (PV) 24 h post-infection and found that most PVs of the
196 *iΔTgCoq1*(+ATc) contained 2 parasites, some with 4 parasites and none with 8 or 16. Under
197 identical conditions, the parental and the complemented mutants showed a similar distribution
198 pattern with PVs containing 8 and 16 parasites (Fig. 3G). These results support an essential role
199 for TgCoq1 in intracellular *T. gondii* replication.
200

201 **A different isoprenoid tail can replace the one synthesized by TgCoq1**

202 The *Trypanosoma cruzi* solanesyl diphosphate synthase (TcSPPS) was previously characterized
203 and shown to synthesize a product with 9 isoprene units (C45) (25). We wondered if the length of
204 the isoprenoid chain was important for the biological function of UQ in *T. gondii* so we next
205 complemented the *iΔCoq1* mutant with the *TcSPPS* gene (Fig. 4A). Since TgCoq1 localizes to the
206 mitochondrion, we created a construct with the sequence of the N-terminal signal peptide from
207 TgCoq1 and inserted it upstream to the *TcSPPS* gene (Fig. 4A). Southern blot analysis confirmed
208 the presence of the *TcSPPS* gene in the *iΔCoq1-tcspps* mutant (Fig. S4B). Western blot analysis
209 with αHA antibodies show a band at 58 kDa which disappears upon ATc treatment for 3 days.
210 This band also decreased in cells complemented with *TcSPPS* upon treatment with ATc, while the
211 band corresponding to TcSPPS (56 kDa) did not (Fig. S4C). Further validation for the expression
212 of TcSPPS was done with western blots using an anti-TgCoq1 antibody generated against the
213 whole recombinant protein (Fig. 4B). The 58 kDa band is absent in the *iΔCoq1* mutant after
214 culturing with ATc, but is present in the complemented mutant. This anti-TgCoq1 antibody does
215 not react against the TcSPPS and it does not show a reaction in the *iΔCoq1-tcspps* (+ATc). The
216 IFAs in Fig. 4C show the localization of TcSPPS to the mitochondria of the *iΔCoq1-tcspps* mutant,
217 as detected by co-localization with antibodies against TOM40 (30).
218 The severe growth phenotype of the *iΔCoq1(+ATc)* (~5 % of control at 7d +ATc) was reverted
219 by complementation of the mutant with TcSPPS (Fig. 4D), supporting equivalent function of the

220 *T. cruzi* enzyme to TgCoq1 (Fig. 4E-F). A plaquing efficiency assay in which contact between
221 parasites and host cells was limited to 30 min and the number of plaques enumerated (Fig. 4G)
222 showed that TcSPPS expression rescued the phenotype of the *iΔCoq1(+ATc)* mutant. Both plaque
223 size and number were restored by complementation with the TcSPPS enzyme (Fig. 4G).
224 Collectively, these data show that TgCoq1 is essential for *T. gondii* growth, and the length of
225 the isoprenoid unit is not critical for its biological function.
226

227 **TgCoq1 is essential for mitochondrial function**

228 The mitochondrion of *T. gondii* is critical for replication and UQ is essential for the function of
229 the mitochondrial ETC. Considering that UQ is attached to the mitochondrial membrane through
230 the isoprenoid unit synthesized by Coq1, we next investigated whether the *iΔTgCoq1* (+ATc)
231 mutant was unable to grow due to mitochondrial malfunction. We tested two important
232 mitochondrial features: Oxygen consumption rate (OCR) and mitochondrial membrane potential
233 (Fig. 5). We measured the rate of oxygen consumption under basal (state 2); ADP stimulated (state
234 3, oxidative phosphorylation); oligomycin-inhibited (state 4, minimum oxidative
235 phosphorylation), and FCCP-stimulated (state 3u, uncoupled) conditions using digitonin-
236 permeabilized parasites suspended in a buffer containing succinate as substrate (Fig. 5A, see
237 scheme in Fig. S5). Mitochondrial activity of the *iΔTgCoq1* (+ATc) mutant showed significantly
238 lower basal OCR, Ox. Phos (+ADP) and min. Ox. Phos. (+ oligomycin) (Fig. 5B-C). Interestingly,
239 respiration of the TcSPPS-complemented mutant was significantly higher, which could be the
240 result of either higher expression or activity of TcSPPS, or both.
241 We further characterized mitochondrial function by measuring the membrane potential ($\Delta\Psi_m$)
242 of digitonin-permeabilized tachyzoites (controls and mutants) in the presence of succinate as
243 substrate, using safranine O (31). Upon digitonin permeabilization, safranine O is inserted into
244 energized mitochondrial membranes and causes fluorescence quenching. Once a steady state is
245 reached, addition of ADP stimulates synthesis of ATP by the ATP synthase, which uses the H^+
246 gradient, causing a partial depolarization of the membrane and release of safranine O (Fig. 5D).
247 The fluorescence returned to its basal level upon addition of oligomycin, which inhibits ATP
248 synthase activity and prevents further depolarization by ADP. FCCP addition uncoupled oxidative
249 phosphorylation releasing safranine O (Fig. 5D). The *iΔCoq1* (+ATc) mutant was unable to load
250 safranine up to the same level as the controls, indicating partial depolarization of the mitochondrial

251 membrane potential (Fig. 5D and E). Complementation with TgCoq1 or TcSPPS restored
252 mitochondrial membrane potential to the same level as the parental controls.
253 These results showed that TgCoq1 is essential for mitochondrial function in *T. gondii*, which
254 was restored after complementation.
255

256 **The lipophilic bisphosphonate BPH-1218 inhibits TgCoq1 and protects mice against *T.***
257 ***gondii* infection**

258 Previous work has shown that bisphosphonates can target several enzymes of the isoprenoid
259 biosynthesis pathway, including the farnesyl diphosphate synthase (FPPS) which synthesizes FPP,
260 the preferred substrate of TgCoq1 (14). We screened for potential inhibitors that could specifically
261 inhibit TgCoq1 and tested a series of ~200 bisphosphonates. We measured the IC_{50}s for the most
262 promising candidates and in parallel we evaluated the inhibition of the recombinant TgCoq1 and
263 recombinant TgFPPS, for comparison (Table 2). One interesting compound (BPH-1218) was more
264 effective at inhibiting TgCoq1 than TgFPPS, with an IC_{50} of 36 nM for the inhibition of TgCoq1
265 and an EC_{50} of 0.92 μM against *T. gondii* growth *in vitro* (Table 2). We further determined
266 specificity against TgCoq1, by comparing the growth inhibition of the compound against a parental
267 strain (RH) versus a cell line over-expressing TgCoq1 (*TgCoq1-OE*). BPH-1218 (Fig. 6A), appears
268 to specifically target TgCoq1, as supported by the 3-fold increase in EC_{50} against *TgCoq1-OE*
269 compared to the parental strain (Fig. 6B, and Table 3). BPH-1218 was shown before to inhibit the
270 TcSPPS with an IC_{50} of 60 nM and cause a 40% decrease in UQ_9 biosynthesis in *T. cruzi* (32).
271 BPH-1218 showed very little toxicity when tested against human fibroblasts cells (Supplementary
272 Table S3).
273 We next tested BPH-1218 *in vivo* in Swiss webster mice infected with 100 tachyzoites of the
274 RH strain. We started treatment with BPH-1218 six hours post-infection and administered the drug
275 daily for 10 days. We observed that BPH-1218 was protective against acute *T. gondii* infection *in*
276 *vivo* with a ED_{50} of 0.69 mg/kg/day (Fig. 6D). The initial infection was successful as shown by the
277 resistance to re-infection of the surviving mice (Fig. 6E). The protection by BPH-1218 was further
278 shown in a model of dissemination of the infection for which we infected mice with a strain of *T.*
279 *gondii* that expresses a luciferase gene (a gift from Jeroen Saiej) that enables measurement of the
280 level of infection in live mice with an IVIS illumination system (33). Treatment with BPH-1218
281 showed a remarkable effect on both virulence and dissemination of the infection (Fig. 6F-G).

282 In summary, both *T. gondii* growth *in vitro* and mice virulence were blocked by
283 pharmacological inhibition of TgCoq1.
284
285 **An UQ derivative rescues BPH-1218 growth inhibition and *iΔCoq1* (+ATc) growth defect**
286 To further validate the role of TgCoq1 in the synthesis of ubiquinone we tested if supplementing
287 cultures of the *iΔCoq1* (+ATc) mutant with various ubiquinones would rescue the growth defect
288 (Fig. 7). Because UQ_7 is not commercially available we tested UQ_6, UQ_8 and CoQ_{10} and observed
289 a remarkable rescue of the growth of the *iΔCoq1*(+ATc) mutant by UQ_6 (Fig. 7A). The other UQs
290 did not have a significant effect and could be the result of poor solubility or permeability (Fig. 7B).
291 We next wondered if UQ_6 would rescue the growth inhibition by BPH-1218 (Fig. 7C-D). UQ_6
292 was able to rescue both genetic and pharmacological inhibition of TgCoq1. We applied this
293 strategy with a larger number of compounds and tested % growth of 18 known mitochondrial
294 inhibitors (shown in Table S4) and their possible rescue by UQ_6 (Fig. 7E, at 2x and 4x EC_{50}s). We
295 observed that for some compounds the % growth did not change by adding UQ_6 to the culture but
296 some of them showed a reduced inhibitory effect. We next seleced five compounds and determined
297 their EC_{50} in the presence of UQ_6 , and we observed that for three of them (BPH-1218, BPH-1217
298 and BPH-1236) the EC_{50} was increased when the cultures were supplemented with UQ_6 (Table 4).
299 The growth inhibition by JAG21, a highly effective mitochondrial inhibitor (34), was not rescued
300 by UQ_6 but there was a modest rescue by the mitochondrial inhibitor atovaquone (Fig. 7E).
301 In summary, TgCoq1 is an essential enzyme that forms part of the ubiquinone biosynthesis
302 pathway and its pharmacological inhibition represents a new target that can be blocked with known
303 bisphosphonates. Ubiquinone biosynthesis is an unexplored target in apicomplexan parasites and
304 our work shows a strategy to discover new inhibitors via rescue with ubiquinones.
305

306 **DISCUSSION**

307

308 In this work we report the characterization of a polyprenyl diphosphate synthase *TGGT1_269430*
309 (35) (TgCoq1), the first enzyme of the ubiquinone synthesis pathway in *Toxoplasma gondii*.
310 TgCoq1 localizes to the mitochondrion of *T. gondii* and is essential for parasite growth and
311 infectivity. We showed that TgCoq1 synthesized heptaprenyl diphosphate (C35) and *T. gondii*
312 produces UQ_7. TgCoq1 was essential for normal mitochondrial function and both mitochondrial

313 respiration and membrane potential were negatively impacted after genetically downregulating the
314 expression of *TgCoq1*. We also show that over-expression of TgCoq1 protected parasite growth
315 from the inhibitory effect of the lipophilic bisphosphonate BPH-1218. Supplementation with UQ_6
316 rescued both the retarded growth of the conditional mutant and the inhibition by the
317 bisphosphonate. The bisphosphonate also protected mice infected with a lethal dose of *T. gondii*
318 at an ED_{50} of 0.69 mg/kg/day.

319 Ubiquinones consist of a water-soluble (*p*-quinone/*p*-dihydroxyphenyl) headgroup that can
320 accept or donate two electrons to the respiratory chain, and a lipophilic isoprenoid tail that targets
321 the molecule to membranes. The isoprenoid tail is essential for the function of UQs in the electron
322 transport chain of mitochondria (36). The isoprenoid unit is derived from a common precursor,
323 isopentenyl pyrophosphate (IPP), and its isomer, dimethylallyl pyrophosphate (DMAPP), which
324 are synthesized in mammalian cells via the mevalonate pathway, but in *T. gondii* are synthesized
325 via the apicoplast-localized methylerythritol phosphate (MEP) pathway (Fig. 1A), which is
326 essential (7). In *T. gondii*, IPP and DMAPP are condensed by the action of an unusual farnesyl
327 diphosphate synthase (TgFPPS) into farnesyl diphosphate (FPP) and geranylgeranyl diphosphate
328 (GGPP) (14). Previous work from our group demonstrated that *T. gondii* imports FPP and GGPP,
329 from the host cell, making them sensitive to host isoprenoid biosynthesis inhibitors, but at the same
330 time less vulnerable to inhibitors of the parasite enzymes (15). FPP and GGPP are further elongated
331 by long-chain prenyl diphosphate synthases, and their products play important roles in the
332 synthesis of essential molecules such as ubiquinones, menaquinones, some hemes, hormones, and
333 vitamins. Very little is known about the role of the longer-chain isoprenoid biosynthesis enzymes
334 in *T. gondii*.

335 The number of isoprenyl units that are incorporated into the tail of UQ differ between species
336 (6), for example, *P. falciparum* synthesizes UQ_8 (37) while humans synthesize UQ_{10}, and *T. cruzi*
337 synthesizes UQ_9 (25). The synthesis of UQ and its insertion in the mitochondrial membrane is
338 unexplored in *T. gondii* or any other apicomplexan parasite. Considering that the mitochondrion
339 of *T. gondii* and also of other apicomplexan parasites is critical for their replication and several
340 major antiparasitic drugs, such as atovaquone (38) and endochin-like quinolones (39), inhibit the
341 mitochondrial electron transport chain at the coenzyme Q:cytochrome c reductase, we explored
342 TgCoq1 as a potential target for chemotherapy. Endochin-like quinolones target mitochondrial
343 respiration, and they were found to eliminate tissue cysts at ~76-88% of the control (40).
344 Bisphosphonates represent a promising class of drug candidates and they have been used

345 previously to treat other human diseases like osteoporosis (11). Work from our laboratory and
346 others have shown that the isoprenoid pathway is a validated target for controlling *Toxoplasma* (7,
347 14, 41-45), *Plasmodium spp.*(41, 46-48) and *Cryptosporidium* (49).
348 Screening of several bisphosphonate derivatives yielded the lipophilic bisphosphonate BPH-
349 1218 that inhibited the activity of TgCoq1 and *in vitro* growth of *T. gondii*. In addition, BPH-1218
350 protected mice against a lethal infection with *T. gondii*. Targeting of TgCoq1 by BPH-1218 was
351 underscored by several pieces of evidence. First the sensitivity of the recombinant enzyme with an
352 IC_{50} of 60 nM; second, overexpression of the *TgCoq1* gene resulted in parasites more resistant to
353 its inhibition; third, the inhibition of growth was rescued by the UQ derivative UQ_6, the EC_{50} of
354 BPH-1218 increasing when an ubiquinone was added to the culture. Compared with other
355 compounds which also showed increased EC_{50} in the presence of UQ_6, BPH-1218 was the only
356 one for which the protection against inhibition by UQ_6 was large—almost 8 times.
357 In conclusion, we present a new *T. gondii* target, TgCoq1, that can be inhibited by specific
358 compounds that are neither toxic nor affect host cell growth. Inhibition of TgCoq1 impacted
359 mitochondrial activity, a validated target in all apicomplexans. The ubiquinone synthesis pathway
360 emerges as a novel and unexplored pathway suitable for new chemotherapeutic approaches.
361
362 **MATERIALS AND METHODS**
363
364 **Ethics Statement**
365 All animal care and therapy studies were carried out in accordance with the NIH guidelines. The
366 animal use protocol was reviewed and approved by the Institutional Animal Care and Use
367 Committee (IACUC) of the University of Georgia. AUP# A2018 02-021.
368
369 **Phylogenetic Analysis**
370 The protein sequences were retrieved from the National Center for Biotechnology Information
371 (NCBI) database. The phylogenetic tree from Li et al (50) was used as a guide to search for known
372 solanesyl diphosphate synthases (SPPS), hexaprenyl diphosphate synthases (HexPPS), and other
373 long chain prenyl diphosphate synthases. The *T. gondii* Coq1 sequence was used to query the
374 NCBI database using the genomic Basic Local Alignment Search Protein (BLASTP) tool by
375 selecting organisms ranging from prokaryotes to eukaryotes. The default BLAST parameters

376 (expected threshold: 10, low-complexity filter, BLOSSUM 62 substitution matrix) were used.
377 Alignments for phylogenetic trees were constructed using phylogeny.fr website (51, 52). Protein
378 sequences were inputted to create multiple sequence alignments using the ClustalW program with
379 the auto strategy settings (53). The alignments were then trimmed manually to trim the extended
380 N-terminals of the TgCoq1, HhPPS, and the SnPPS. The trimmed sequence alignments were then
381 used to create a maximum likelihood tree through Molecular Evolutionary Genetics Analysis
382 (MEGA) with the Jones-Taylor-Thornton (JTT) matrix-based model (54) with 1000 bootstraps
383 and branch lengths measured in the number of substitutions per site (55, 56).
384

385 **Chemicals and reagents**

386 Oligonucleotide primers were obtained from Integrated DNA Technologies (IDT). Taq DNA
387 polymerases were from Denville Scientific Inc. and Invitrogen. TRIzol reagent, SuperScript TM
388 III Reverse Transcriptase, TOPO TA cloning kit, and GeneRacer™ Advanced RACE Kit were
389 from Invitrogen and dNTP were from New England BioLab Inc. Restriction enzymes were from
390 New England BioLab Inc. and Promega. Plasmid miniprep kit, Gel extraction kit and DNA
391 purification kit were from Zymo Research. Secondary antibodies with fluorescence for the western
392 blots are from Licor. IPP, DMAPP, GPP, FPP, GGPP were from Sigma. [4-^{14}C] Isopentenyl
393 diphosphate triammonimum salt (55.0 mCi/mml) was from PerkinElmer Life Sciences.
394 Ubiquinone Q6 (UQ_6) and Q8 (UQ_8) were from Avanti Polar Lipids. Ubiquinone Q10 (UQ_{10}) was
395 from Sigma-Aldrich. Silica gels HPTLC were from Analtech. All other reagents were analytical
396 grade or better.
397

398 **Cultures**

399 *T. gondii* RH strain tachyzoites were cultured using hTERT (human telomerase reverse
400 transcriptase) cells with 1% BCS and purified as described earlier (57, 58). Host cells were grown
401 in Dulbecco's modified minimal essential medium supplemented with 10 % cosmic calf serum.
402 Cell cultures were maintained at 37°C with 5 % CO_2.
403

404 **Protein Studies and Enzymatic Determinations**

405 The expression cassette was introduced into *E. coli* BL21-Codon (+) cells. The transformed *E. coli*
406 were selected with Kanamycin. Expression of the recombinant protein was optimally induced by

407 adding 0.4 mM isopropyl β-thiogalactopyranoside (IPTG) to the culture at an OD_{600} of 0.5-0.8.
408 The bacterial culture was grown overnight at 18°C. A HisBind 900 cartridge from Novagen was
409 used to purify the recombinant protein as per the manufacturer's instructions. The purified protein
410 was desalted using a His Trap Desalting columns from GE Healthcare according to the prescribed
411 protocol and was stored at -80°C with 40 % glycerol.
412 Kinetic parameters for the recombinant TgCoq1 were calculated from the activity obtained by
413 varying the concentration of the allylic substrates (GPP, FPP, GGPP and IPP) and keeping
414 concentration of counter substrates at a saturating level. The nonlinear regression analysis in Sigma
415 plot 10.0 was used to calculate the Kinetic parameters.
416 For the enzymatic activity, a standard protocol for medium/long chain prenyl diphosphate
417 synthase was followed as described previously (25). The enzyme activity was measured by
418 assessing the amount of [4-^{14}C] IPP incorporated into butanol-extractable polyprenyl
419 diphosphates. The standard assay mixture contained, in a final volume of 100 µL, Tris-HCl (100
420 mM, pH 7.4) 100 µM of any of the allylic substrates FPP/GGPP/GPP, 1 mM $MgCl_2$,1 mM DTT,
421 1 % v/v Triton X-100, 100 µM [4-^{14}C]-IPP (1 µCi/µMol) and 500 ng of purified protein. Reactions
422 were incubated at 37°C for 30 min unless otherwise indicated. The radioactive prenyl products
423 were extracted with 1-butanol, washed with NaCl-saturated water and activities were calculated
424 from the DPM values.
425
426 **Product analysis by reverse phase thin-layer chromatography**
427 The radioactive prenyl diphosphate products were extracted from 500 µL reaction and hydrolyzed
428 to their corresponding alcohols (polyprenols) by using potato acid phosphatase. The enzymatic
429 hydrolysis reaction was set at 37°C for more than 12 hours as described before (16). The resultant
430 products were extracted with n-pentane and separated on a reverse-phase TLC plate with
431 acetone:water (19:1 v/v) as the solvent system. The positions of the polyprenol standards were
432 visualized by iodine vapors and marked with pencils. The radioactive polyprenol products were
433 exposed and visualized by autoradiography.
434
435 **Extractions and UQ_7 measurements**
436 Ubiquinone (UQ) from *T. gondii* was isolated using a standard modified protocol as follows, (6).
437 Parasites were collected and purified by filtration through an 8 µM, 5 µM, and 3 µM nucleopore

438 membrane, followed by two wash steps in Buffer A with glucose (116 mM NaCl, 5.4 mM KCl,
439 0.8 mM $MgSO_4.7H_2O$, 50 mM HEPES, 5.5 mM Glucose), and resuspended in a hypoosmotic
440 buffer (20 mM HEPES-Tris pH 7.4, 1 mM EDTA) and centrifuged. The final parasite pellet was
441 subject to 4 freeze-thaw cycles of liquid nitrogen for 5 min and 37°C for 1 minute, to lyse cells.
442 The cell pellet was resuspended in 500 µl of a 1-propanol:water (3:1) followed by 2 cycles of 60
443 s of grinding with glass beads (425-600 µm). The slurry was transferred to a tube and an additional
444 500 µl of the 1-propanol:water plus 500 µl of n-hexane was added to extract the UQ, vortexed,
445 and centrifuged at 13,000 rpm for 5 minutes. The upper phase containing the UQ was collected
446 into a glass tube and the grinding was repeated. The UQ containing phase was dried under Nitrogen
447 gas and analyzed by TLC and HPLC.
448
449 **TLC, HPLC and Mass Spec analysis**
450 The UQ extract was analyzed by normal-phase thin layer chromatography (TLC) with authentic
451 UQ_6, UQ_8 and UQ_{10} standards. The samples of UQ extracts were solubilized in
452 chloroform/methanol (2:1, v/v) for spotting. Normal-phase TLC was conducted on a Kieselgel 60
453 F_{254} plate (Merck Millipore) and was developed with benzene for separation for 1 hour. The plate
454 was viewed under UV illumination, the UQ band was collected, and the sample was extracted with
455 hexane/isopropanol (1:1, v/v). Samples were vacuum-dried at 50°C and solubilized in ethanol.
456 Purified UQ was subjected to high-performance liquid chromatography on a Shimadzu HPLC
457 Class VP series equipped with a reverse phase YMC-Pack ODS-A column (YMC). Ethanol was
458 used as the mobile phase at a flow rate of 1.0 mL/min, and detection was performed by monitoring
459 absorption at 275 nm. Toxoplasma UQ_7 was pinpointed comparing with UQ_7 standard directly
460 obtained and purified from *E. coli* harboring heptaprenyl diphosphate synthase gene of *H.*
461 *influenzae* (*E. coli* KO229/pMN18).
462 The quantification of UQ_7 of toxoplasma was done by using 10 µg of UQ_{10} as an internal
463 control. UQ_7 and UQ_{10} were co-purified with hexane/isopropanol (1:1, v/v). The quantification of
464 UQ_7 was calculated based on the peak area of UQ_7 and UQ_{10} in the HPLC chromatogram and cell
465 numbers of parasites.
466 For LC/MS analysis, toxoplasma UQ_7 extract was solubilized with methanol/isopropanol
467 (4:1 v/v) with 0.01 µM of ammonium formate and subjected to Waters Xevo TQMS coupled with
468 Acquity UPLC system with Acquity UPLC BEH C18 column. Methanol/isopropanol (4:1 v/v)

469 with 0.01 μM of ammonium formate was used as mobile phase at the flow rate of 0.3 mL/min.
470 The detection was performed by monitoring absorption at 275 nm PDA (photo diode array), and
471 total ion chromatogram (TIC) was extracted for specific UQ_7 peak (MS scan). The MS spectra
472 showed the specific m/z value of UQ_7 in the form of ammonium adduction.
473
474 **Genetic manipulations**
475 For *in situ* tagging, a fragment of approximately 2 kbs was amplified from the genomic locus (3'
476 region) of the *TgCoq*1 gene using primers 1 and 2 (Table S5). The fragment was cloned in the pLic-
477 3HA-CAT plasmid (27) and the construct was linearized with *NheI* for transfection of *TatiΔku80*
478 parasites. Clonal cell lines were generated after selection and subcloning and termed *TgCoq1-3HA*.
479 A promoter insertion plasmid was generated by cloning two fragments from the 5' end of the *TgCoq1*
480 gene into the pDT7S4myc plasmid (27). One fragment corresponds to the *TgCoq1* 5' flanking region
481 (predicted promoter/5'UTR) and was amplified with primers 3 and 4 (Table S6, underlined sequences
482 correspond to *NdeI* restriction sites). The second fragment corresponds to the 5' *TgCoq1* coding
483 sequence beginning with the start codon, which was amplified with primers 5 and 6 (Table S6)
484 (underlined sequences correspond to BglII and AvrII restriction sites). The plasmid was linearized
485 with AvrII for transfection of *TatiΔku80* and *TgCoq1-3HA* cells. The clonal lines created after
486 selection and subcloning were termed *iΔCoq1* and *iΔCoq1-3HA*.
487 The full-length cDNA of *TgCoq1* was amplified with primers TgCoq1-PI-BGLII-F (primer 6)
488 and TgCoq1-PI-AVRII-R (primer 7). The RT-PCR product was cloned in the Zero blunt Topo
489 vector from Invitrogen. After the sequence was verified, the *TgCoq1* ORF was removed by
490 digestion with BglII and AvrII, cloned into the BglII and AvrII sites of pCTH3 (59) to generate
491 the **pCTCoq1HA** plasmid for complementation. Cosmid **PSBME30** (toxodb.org), which contains
492 the *TgCoq1* genomic locus was obtained from Dr. L. David Sibley (Washington University). For
493 the complementation with the *Trypanosoma cruzi* solanesyl diphosphate synthase (TcSPPS), 453
494 bp of the 5' end of the *TgCoq1* ORF was fused with the cDNA of TcSPPS, and the pCTH3 vector
495 by Gibson Assembly to make the p**CTSPPSHA** construct. These three constructs were used for
496 complementation of the conditional knockout cells. The complemented cells were selected by
497 ATc. After surviving ATc selection, the cells were subcloned by limiting dilution. The single
498 clones were analyzed by PCR, and confirmed by Southern blot.
499

500 **Immunofluorescence (IFA), western blots, and Southern blots**

501 For IFAs of intracellular parasites subconfluent HFF host cells were used and infected with
502 tachyzoites for 24 hours and fixed with 3% paraformaldehyde. For IFAs of extracellular parasites,
503 *T. gondii* tachyzoites were released by lysing hTERT cells and fixed in 3% paraformaldehyde for
504 1 h at room temperature. Parasites were adhered to poly-L-Lysine coated cover slips. In both cases
505 parasites were permeabilized with 0.3 % Triton X-100 for 30 min and blocked with blocking buffer
506 (3 % Bovine serum albumin). Incubations with primary and secondary antibodies were for 1 h
507 each. Primary anti-HA antibodies were used at a dilution of 1:200. Secondary antibodies, in all
508 cases, were used at a concentration of 1:1,000. Cover slips with parasites were mounted on glass
509 slides with Antifade-DAPI. A Delta Vision fluorescence microscope was used to observe cells and
510 a Photometrics Coolsnap camera to capture images. Deconvolved images were obtained by using
511 softWoRx deconvolution software.

512 For western blots, separated proteins in SDS page were transferred to a nitrocellulose
513 membrane and blocked overnight at 4°C with 5 % nonfat milk in PBS-T (0.1 % Tween-20 in PBS).
514 The protein bands were developed by autoradiography on an X-ray film using an ECL detection
515 kit or imaged on a Licor Odyssey CLx machine using secondary antibodies with fluorescence at
516 either 680 or 800 nm.

517 *T. gondii* genomic DNA was purified and digested with EcoRI or EcoRV for Southern blot
518 analysis. The probe used in Southern blot is the purified PCR product of the 453 bp fragment at
519 the 5' of TgCoq1 cDNA. The probe was labeled with ^{32}P by random priming.

520

521 **TgCoq1 antibody production**

522 The TgCoq1 recombinant protein was generated with a *E. coli* expression system and the whole
523 gene was cloned in the pET-28a (+) vector. The *TgCoq1* coding region was released from the pCR-
524 2.1-TOPO vector by digestion with NcoI and NotI and ligated into the NcoI and NotI sites of the
525 pET-28a (+) vector. The resultant pET-28a (+)-TgCoq1 expression construct was modified with a
526 C-terminal 6x His-tag to produce a His-tagged fusion protein. The construct was sequenced and
527 used for transformation of *E. coli* BL21 codon plus. Purified protein (100 μg) was first mixed with
528 Freund's complete adjuvant and used to inoculate mice which were boosted three times 2 weeks
529 apart with 50 μg peptide in Freund's incomplete adjuvant (60, 61). The final serum was tested on
530 *Coq1-HA* lysates and compared with anti-HA to confirm size and antibody purity. The anti-Coq1

531 serum was affinity purified prior to use for IFAs and westerns. Work with mice was carried out in
532 strict accordance with the Public Health Service Policy on Humane Care and Use of Laboratory
533 Animals and Association for the Assessment and Accreditation of Laboratory Animal Care
534 guidelines. The animal protocol was approved by the University of Georgia's Committee on the
535 Use and Care of Animals (protocol A2018 02-021). All efforts were made to humanely euthanize
536 the mice after collecting blood.
537

538 **Plaque assays and plaquing efficiency**

539 Plaque assays were performed with confluent hTERT cells in six-well plates infected with 150
540 parasites per well and incubated with or without ATc (61). After 8 days of incubation, parasites
541 were fixed with 100% ethanol and stained as previously described (62). ImageJ software was used
542 for quantification of plaque size. Fifteen plaques per well for each biological replicate were
543 counted and averaged. Plaquing efficiency assays were performed with confluent hTERT host
544 cells in six-well plates infected with 2,000 parasites per well. Parasites were preincubated for 3
545 days with ATc, and then incubated with or without ATc. Thirty minutes after inoculation parasites
546 are washed off with PBS and replaced with fresh DMEM media. After 5 days of incubation the
547 parasites were fixed and stained using the same protocol as the plaque assays. The number of
548 plaques were counted and averaged from 3 biological replicates.
549

550 **Measuring mitochondrial membrane potential and oxygen consumption**

551 The mitochondrial membrane potential was measured by the safranine method according to (31)
552 and (34). Freshly lysed parasites were collected and filtered through an 8 µm filter to remove host
553 cell debris. The parasites were washed twice with BAG and resuspended at 1 x 10^9 parasites per
554 ml. An aliquot of 50 µl of the parasite suspension (5 x 10^7 cells) was added to a cuvette containing
555 Safranine O (2.5 µM) and succinate (1 mM) in 2 ml of reaction buffer (125 mM sucrose, 65 mM
556 KCl, 10 mM HEPES-KOH pH 7.2, 1 mM $MgCl_2$, and 2.5 mM K_3PO_4 pH 7.2). The cuvette was
557 placed in a Hitachi F-7000 fluorescence spectrophotometer and digitonin (30 µM) was added to
558 selectively permeabilize the plasma membrane. The cells were then allowed to equilibrate, and
559 ADP (10 µM final) was added to stimulate oxidative phosphorylation and oligomycin (2 µg/ml
560 final) to inhibit the ATP synthase. FCCP (5 µM) was used to depolarize the mitochondrial
561 membrane. The quantification of the mitochondrial membrane potential is the difference of the

562 maximum fluorescence (after addition of FCCP) minus the minimum fluorescence (before addition
563 of ADP).
564 Measurements of oxygen consumption are performed with an Oroboros O_2kFluoRespirometer
565 and the data was analyzed using DatLab software and GraphPad Prism 7 following a published
566 protocol (63). The parasites were collected using the same protocol described above for
567 mitochondrial membrane potential. 5 x 10^7 parasites were loaded into the chamber with succinate
568 (5 mM), BSA (0.2%), EGTA (50 μM) in 2 ml of reaction buffer (125 mM Sucrose, 65 mM KCl,
569 10 mM HEPES-KOH, 2.5 mM potassium phosphate). The chamber was closed to minimize the
570 effects of oxygen from the environment and the suspension was allowed to equilibrate for 10
571 minutes. Digitonin (12.5 μM) was added and the suspension allowed to equilibrate for 10 min,
572 then ADP (200 μM) was added followed by oligomycin (1.5 μM) after 5-6 min. The quantification
573 in Fig. 5C shows the average peaks after each addition of drug for 3 biological replicates for each
574 cell type. The basal levels represent the normal oxygen consumption of the mitochondria after
575 digitonin. The Ox. Phos. represents the average oxidative phosphorylation after the addition of
576 ADP. The Min. Ox. Phos. represents the minimum oxidative phosphorylation after the addition of
577 oligomycin.
578

579 ***In vitro* drug screening and growth assays**

580 To test the effect of bisphosphonates on TgCoq1 activity, enzymatic reactions were set up in the
581 presence of different bisphosphonate compounds. Preliminary screening for potential inhibitors
582 was carried out at a final concentration of 1 μM and 10 μM, respectively and IC_{50}s were calculated
583 for the ones that showed > 50% inhibition at 1 μM. The protocol used was previously described
584 (64).
585 Experiments on *T. gondii* tachyzoites were carried out using parasites expressing red
586 fluorescent protein (RFP) (65) with the modification described by Recher et al (66). Tachyzoites
587 were maintained in human fibroblasts (hTERT cells). For drug testing and growth assays, parasites
588 were purified by passing them through a 25-gauge needle, followed by filtration through a 3 μm
589 filter. Human fibroblasts were cultured in 96-well black sided plates for 24 hours prior to the
590 addition of 4,000 fluorescent tachyzoites/well. Fluorescence values were measured for up to 9
591 days, and both excitation (544 nm) and emission (590 nm) were read from the bottom of the plates
592 in a Molecular Devices plate reader (45). The EC_{50}s were calculated using Prism software. The

593 UQ_6 experiments were performed using the same protocol as described above. The parasites were
594 supplemented with 10 μM UQ_6. The drug compounds were tested at 2X or 4X their known EC_{50}
595 values.
596
597 **Cytotoxicity to hTert cells.** The cytotoxicity was tested using an alamarBlue assay as described
598 by Recher et al. (66). Toxicity was not high enough at the concentrations of drugs tested for
599 detection with alamarBlue.
600
601 ***In vivo* drug screening**
602 Experiments were carried out as described previously (48) using 100 *T. gondii* tachyzoites of the
603 RH strain to infect Webster mice. Drugs were dissolved in 10% kolliphor HS 15 and were
604 inoculated intraperitoneally (i.p.). Treatment was initiated 6 hours after infection and administered
605 daily for 10 days.
606 For the imaging experiments, 20 *T. gondii* tachyzoites of the RH strain (RH-cLuc-GFP, a gift
607 from Saeij lab) were used to infect Webster mice. Treatment protocol was similar to the described
608 above. *In vivo* imaging of infected animals was performed at day 8. The δ-Luciferin potassium salt
609 (Gold Biotech) was dissolved at a concentration of 15.4 mg/ml in sterile PBS. 200 ml of this δ-
610 Luciferin potassium salt solution was injected into each mouse via an intraperitoneal (i.p.) route
611 (33). The mice were anesthetized using 2.5% (vol/vol) gaseous isofluorane in oxygen. Then the
612 mice were imaged on an IVIS 100 imager (Xenogen, Alameda, CA) (67). Quantification of
613 bioluminescence result was performed using Living Image v4.3 software (Xenogen).
614
615 **Statistical Analysis**
616 Experimental data are expressed as the mean values ± standard deviations (SD) from at least three
617 independent experiments unless indicated otherwise. Statistical analyses were performed by
618 Student's t-test using GraphPad PRISM version 8.2. The results of the *in vivo* studies were
619 analyzed using the Kaplan-Meier log rank test (GraphPad Prism 7 software). A P value of < 0.05
620 was considered statistically significant.
621
622

ACKNOWLEDGEMENTS

We thank Rodrigo Baptista for advice on the phylogenetic analysis, Mayara Bertolini for training on the use of the Oroboro, Andrea Hortua Triana for assistance with the generation of the anti-TgCoq1 antibodies. The anti-TOM40 antibodies were a gift from Boris Striepen. The work was funded by NIH grants AI102254 and AI147661 to SNJM. MAS was partly funded through a T32 Training Grant fellowship T32AI060546. MK was funded by a grant-in-aid from the Ministry of Education, Culture, Sports, Science, and Technology of Japan [#21H02117] . EO was supported by the University of Illinois Foundation and by a Harriet A. Harlin Professorship.

AUTHORS CONTRIBUTION

MAS and ZHL performed most experiments, analyzed the data and wrote the manuscript. RB cloned and characterized the recombinant enzyme. BB performed some of the UQ_6 drug testing. CL performed the initial characterization of the mutant. JJ and MK analyzed the toxoplasma extracts for the determination of UQ_7. SRM synthesized all the bisphosphonates and carried out computational structure predictions. EO edited the manuscript. SNJM supervised the project and wrote and edited the manuscript.

REFERENCES

1. Hill D, Dubey JP. 2002. Toxoplasma gondii: transmission, diagnosis and prevention. Clin Microbiol Infect 8:634-40.
2. Weiss LM, Dubey JP. 2009. Toxoplasmosis: A history of clinical observations. Int J Parasitol 39:895-901.
3. Guo M, Mishra A, Buchanan RL, Dubey JP, Hill DE, Gamble HR, Jones JL, Pradhan AK. 2016. A Systematic Meta-Analysis of Toxoplasma gondii Prevalence in Food Animals in the United States. Foodborne Pathog Dis 13:109-18.
4. Alday PH, Doggett JS. 2017. Drugs in development for toxoplasmosis: advances, challenges, and current status. Drug Des Devel Ther 11:273-293.
5. Porter SB, Sande MA. 1992. Toxoplasmosis of the central nervous system in the acquired immunodeficiency syndrome. N Engl J Med 327:1643-8.
6. Okada K, Suzuki K, Kamiya Y, Zhu X, Fujisaki S, Nishimura Y, Nishino T, Nakagawa T, Kawamukai M, Matsuda H. 1996. Polyprenyl diphosphate synthase essentially defines the length of the side chain of ubiquinone. Biochim Biophys Acta 1302:217-23.
7. Nair SC, Brooks CF, Goodman CD, Sturm A, McFadden GI, Sundriyal S, Anglin JL, Song Y, Moreno SN, Striepen B. 2011. Apicoplast isoprenoid precursor synthesis and the molecular basis of fosmidomycin resistance in Toxoplasma gondii. J Exp Med 208:1547-59.
8. Gershenzon J, Dudareva N. 2007. The function of terpene natural products in the natural world. Nat Chem Biol 3:408-14.
9. Imlay L, Odom AR. 2014. Isoprenoid metabolism in apicomplexan parasites. Curr Clin Microbiol Rep 1:37-50.
10. Oldfield E. 2010. Targeting isoprenoid biosynthesis for drug discovery: bench to bedside. Acc Chem Res 43:1216-26.
11. Roelofs AJ, Thompson K, Gordon S, Rogers MJ. 2006. Molecular mechanisms of action of bisphosphonates: current status. Clin Cancer Res 12:6222s-6230s.
12. Johnston S, Wilson K, Varker H, Malangone-Monaco E, Juneau P, Riehle E, Satram-Hoang S, Sommer N, Ogale S. 2017. Real-world Direct Health Care Costs for Metastatic Colorectal Cancer Patients Treated With Cetuximab or Bevacizumab-containing Regimens in First-line or First-line Through Second-line Therapy. Clin Colorectal Cancer 16:386-396 e1.
13. Lange BM, Rujan T, Martin W, Croteau R. 2000. Isoprenoid biosynthesis: the evolution of two ancient and distinct pathways across genomes. Proc Natl Acad Sci U S A 97:13172-7.
14. Ling Y, Li ZH, Miranda K, Oldfield E, Moreno SN. 2007. The farnesyl-diphosphate/geranylgeranyl-diphosphate synthase of Toxoplasma gondii is a bifunctional enzyme and a molecular target of bisphosphonates. J Biol Chem 282:30804-16.
15. Li ZH, Ramakrishnan S, Striepen B, Moreno SN. 2013. Toxoplasma gondii relies on both host and parasite isoprenoids and can be rendered sensitive to atorvastatin. PLoS Pathog 9:e1003665.
16. Koyama T. 1999. Molecular analysis of prenyl chain elongating enzymes. Biosci Biotechnol Biochem 63:1671-6.
17. Liang PH, Ko TP, Wang AH. 2002. Structure, mechanism and function of prenyltransferases. Eur J Biochem 269:3339-54.
18. Saiki R, Nagata A, Kainou T, Matsuda H, Kawamukai M. 2005. Characterization of solanesyl and decaprenyl diphosphate synthases in mice and humans. FEBS J 272:5606-22.

19. Kelley LA, Mezulis S, Yates CM, Wass MN, Sternberg MJ. 2015. The Phyre2 web portal for protein modeling, prediction and analysis. Nat Protoc 10:845-58.
20. Chen C-CM, Satish R.; Han, Xu; Liu, Weidong; Ma, Lixin; Zhai, Chao; Dai, Longhai; Huang, Jian-Wen; Shillo, Alli; Desai, Janish; Ma, Xianqiang; Zhang, Yonghui; Guo, Rey-Ting and Oldfield, Eric 2021. Terpene Cyclases and Prenyltransferases: Structures and Mechanisms of Action. ACS Catalysis 11:290-303.
21. Yokoyama T, Mizuguchi M, Ostermann A, Kusaka K, Niimura N, Schrader TE, Tanaka I. 2015. Protonation State and Hydration of Bisphosphonate Bound to Farnesyl Pyrophosphate Synthase. J Med Chem 58:7549-56.
22. Sasaki D, Fujihashi M, Okuyama N, Kobayashi Y, Noike M, Koyama T, Miki K. 2011. Crystal structure of heterodimeric hexaprenyl diphosphate synthase from Micrococcus luteus B-P 26 reveals that the small subunit is directly involved in the product chain length regulation. J Biol Chem 286:3729-40.
23. Desai J, Liu YL, Wei H, Liu W, Ko TP, Guo RT, Oldfield E. 2016. Structure, Function, and Inhibition of Staphylococcus aureus Heptaprenyl Diphosphate Synthase. ChemMedChem 11:1915-23.
24. Gautier R, Douguet D, Antonny B, Drin G. 2008. HELIQUEST: a web server to screen sequences with specific alpha-helical properties. Bioinformatics 24:2101-2.
25. Ferella M, Montalvetti A, Rohloff P, Miranda K, Fang J, Reina S, Kawamukai M, Bua J, Nilsson D, Pravia C, Katzin A, Cassera MB, Aslund L, Andersson B, Docampo R, Bontempi EJ. 2006. A solanesyl-diphosphate synthase localizes in glycosomes of Trypanosoma cruzi. J Biol Chem 281:39339-48.
26. Saiki R, Nagata A, Uchida N, Kainou T, Matsuda H, Kawamukai M. 2003. Fission yeast decaprenyl diphosphate synthase consists of Dps1 and the newly characterized Dlp1 protein in a novel heterotetrameric structure. Eur J Biochem 270:4113-21.
27. Sheiner L, Demerly JL, Poulsen N, Beatty WL, Lucas O, Behnke MS, White MW, Striepen B. 2011. A systematic screen to discover and analyze apicoplast proteins identifies a conserved and essential protein import factor. PLoS Pathog 7:e1002392.
28. Fox BA, Ristuccia JG, Gigley JP, Bzik DJ. 2009. Efficient gene replacements in Toxoplasma gondii strains deficient for nonhomologous end joining. Eukaryot Cell 8:520-9.
29. Mazumdar J, E HW, Masek K, C AH, Striepen B. 2006. Apicoplast fatty acid synthesis is essential for organelle biogenesis and parasite survival in Toxoplasma gondii. Proc Natl Acad Sci U S A 103:13192-7.
30. van Dooren GG, Yeoh LM, Striepen B, McFadden GI. 2016. The Import of Proteins into the Mitochondrion of Toxoplasma gondii. J Biol Chem 291:19335-50.
31. Vercesi AE, Rodrigues CO, Uyemura SA, Zhong L, Moreno SN. 1998. Respiration and oxidative phosphorylation in the apicomplexan parasite Toxoplasma gondii. J Biol Chem 273:31040-7.
32. Shang N, Li Q, Ko TP, Chan HC, Li J, Zheng Y, Huang CH, Ren F, Chen CC, Zhu Z, Galizzi M, Li ZH, Rodrigues-Poveda CA, Gonzalez-Pacanowska D, Veiga-Santos P, de Carvalho TM, de Souza W, Urbina JA, Wang AH, Docampo R, Li K, Liu YL, Oldfield E, Guo RT. 2014. Squalene synthase as a target for Chagas disease therapeutics. PLoS Pathog 10:e1004114.
33. Saeij JP, Boyle JP, Grigg ME, Arrizabalaga G, Boothroyd JC. 2005. Bioluminescence imaging of Toxoplasma gondii infection in living mice reveals dramatic differences between strains. Infect Immun 73:695-702.

34. McPhillie MJ, Zhou Y, Hickman MR, Gordon JA, Weber CR, Li Q, Lee PJ, Amporndanai K, Johnson RM, Darby H, Woods S, Li ZH, Priestley RS, Ristroph KD, Biering SB, El Bissati K, Hwang S, Hakim FE, Dovgin SM, Lykins JD, Roberts L, Hargrave K, Cong H, Sinai AP, Muench SP, Dubey JP, Prud'homme RK, Lorenzi HA, Biagini GA, Moreno SN, Roberts CW, Antonyuk SV, Fishwick CWG, McLeod R. 2020. Potent Tetrahydroquinolone Eliminates Apicomplexan Parasites. Front Cell Infect Microbiol 10:203.
35. Harb OS, Roos DS. 2020. ToxoDB: Functional Genomics Resource for Toxoplasma and Related Organisms. Methods Mol Biol 2071:27-47.
36. Kawamukai M. 2016. Biosynthesis of coenzyme Q in eukaryotes. Biosci Biotechnol Biochem 80:23-33.
37. de Macedo CS, Uhrig ML, Kimura EA, Katzin AM. 2002. Characterization of the isoprenoid chain of coenzyme Q in Plasmodium falciparum. FEMS Microbiol Lett 207:13-20.
38. Srivastava IK, Rottenberg H, Vaidya AB. 1997. Atovaquone, a broad spectrum antiparasitic drug, collapses mitochondrial membrane potential in a malarial parasite. J Biol Chem 272:3961-6.
39. Winter R, Kelly JX, Smilkstein MJ, Hinrichs D, Koop DR, Riscoe MK. 2011. Optimization of endochin-like quinolones for antimalarial activity. Exp Parasitol 127:545-51.
40. Doggett JS, Nilsen A, Forquer I, Wegmann KW, Jones-Brando L, Yolken RH, Bordon C, Charman SA, Katneni K, Schultz T, Burrows JN, Hinrichs DJ, Meunier B, Carruthers VB, Riscoe MK. 2012. Endochin-like quinolones are highly efficacious against acute and latent experimental toxoplasmosis. Proc Natl Acad Sci U S A 109:15936-41.
41. Martin MB, Grimley JS, Lewis JC, Heath HT, 3rd, Bailey BN, Kendrick H, Yardley V, Caldera A, Lira R, Urbina JA, Moreno SN, Docampo R, Croft SL, Oldfield E. 2001. Bisphosphonates inhibit the growth of Trypanosoma brucei, Trypanosoma cruzi, Leishmania donovani, Toxoplasma gondii, and Plasmodium falciparum: a potential route to chemotherapy. J Med Chem 44:909-16.
42. Yardley V, Khan AA, Martin MB, Slifer TR, Araujo FG, Moreno SN, Docampo R, Croft SL, Oldfield E. 2002. In vivo activities of farnesyl pyrophosphate synthase inhibitors against Leishmania donovani and Toxoplasma gondii. Antimicrob Agents Chemother 46:929-31.
43. Szajnman SH, Garcia Linares GE, Li ZH, Jiang C, Galizzi M, Bontempi EJ, Ferella M, Moreno SN, Docampo R, Rodriguez JB. 2008. Synthesis and biological evaluation of 2-alkylaminoethyl-1,1-bisphosphonic acids against Trypanosoma cruzi and Toxoplasma gondii targeting farnesyl diphosphate synthase. Bioorg Med Chem 16:3283-90.
44. Rosso VS, Szajnman SH, Malayil L, Galizzi M, Moreno SN, Docampo R, Rodriguez JB. 2011. Synthesis and biological evaluation of new 2-alkylaminoethyl-1,1-bisphosphonic acids against Trypanosoma cruzi and Toxoplasma gondii targeting farnesyl diphosphate synthase. Bioorg Med Chem 19:2211-7.
45. Li ZH, Li C, Szajnman SH, Rodriguez JB, Moreno SNJ. 2017. Synergistic Activity between Statins and Bisphosphonates against Acute Experimental Toxoplasmosis. Antimicrob Agents Chemother 61:e02628-16.
46. Singh AP, Zhang Y, No JH, Docampo R, Nussenzweig V, Oldfield E. 2010. Lipophilic bisphosphonates are potent inhibitors of Plasmodium liver-stage growth. Antimicrob Agents Chemother 54:2987-93.

47. Jordao FM, Saito AY, Miguel DC, de Jesus Peres V, Kimura EA, Katzin AM. 2011. In vitro and in vivo antiplasmodial activities of risedronate and its interference with protein prenylation in Plasmodium falciparum. Antimicrob Agents Chemother 55:2026-31.
48. Szajnman SH, Galaka T, Li ZH, Li C, Howell NM, Chao MN, Striepen B, Muralidharan V, Moreno SN, Rodriguez JB. 2017. In Vitro and In Vivo Activities of Sulfur-Containing Linear Bisphosphonates against Apicomplexan Parasites. Antimicrob Agents Chemother 61.
49. Moreno B, Bailey BN, Luo S, Martin MB, Kuhlenschmidt M, Moreno SN, Docampo R, Oldfield E. 2001. (31)P NMR of apicomplexans and the effects of risedronate on Cryptosporidium parvum growth. Biochem Biophys Res Commun 284:632-7.
50. Li ZH, Cintron R, Koon NA, Moreno SN. 2012. The N-terminus and the chain-length determination domain play a role in the length of the isoprenoid product of the bifunctional Toxoplasma gondii farnesyl diphosphate synthase. Biochemistry 51:7533-40.
51. Dereeper A, Audic S, Claverie JM, Blanc G. 2010. BLAST-EXPLORER helps you building datasets for phylogenetic analysis. BMC Evol Biol 10:8.
52. Dereeper A, Guignon V, Blanc G, Audic S, Buffet S, Chevenet F, Dufayard JF, Guindon S, Lefort V, Lescot M, Claverie JM, Gascuel O. 2008. Phylogeny.fr: robust phylogenetic analysis for the non-specialist. Nucleic Acids Res 36:W465-9.
53. Thompson JD, Higgins DG, Gibson TJ. 1994. CLUSTAL W: improving the sensitivity of progressive multiple sequence alignment through sequence weighting, position-specific gap penalties and weight matrix choice. Nucleic Acids Res 22:4673-80.
54. Jones DT, Taylor WR, Thornton JM. 1992. The rapid generation of mutation data matrices from protein sequences. Comput Appl Biosci 8:275-82.
55. Kumar S, Nei M, Dudley J, Tamura K. 2008. MEGA: a biologist-centric software for evolutionary analysis of DNA and protein sequences. Brief Bioinform 9:299-306.
56. Kumar S, Stecher G, Li M, Knyaz C, Tamura K. 2018. MEGA X: Molecular Evolutionary Genetics Analysis across Computing Platforms. Mol Biol Evol 35:1547-1549.
57. Moreno SN, Zhong L. 1996. Acidocalcisomes in Toxoplasma gondii tachyzoites. Biochem J 313 (Pt 2):655-9.
58. Vella SA, Calixto A, Asady B, Li ZH, Moreno SNJ. 2020. Genetic Indicators for Calcium Signaling Studies in Toxoplasma gondii. Methods Mol Biol 2071:187-207.
59. Miranda K, Pace DA, Cintron R, Rodrigues JC, Fang J, Smith A, Rohloff P, Coelho E, de Haas F, de Souza W, Coppens I, Sibley LD, Moreno SN. 2010. Characterization of a novel organelle in Toxoplasma gondii with similar composition and function to the plant vacuole. Mol Microbiol 76:1358-75.
60. Chasen NM, Asady B, Lemgruber L, Vommaro RC, Kissinger JC, Coppens I, Moreno SNJ. 2017. A Glycosylphosphatidylinositol-Anchored Carbonic Anhydrase-Related Protein of Toxoplasma gondii Is Important for Rhoptry Biogenesis and Virulence. mSphere 2.
61. Stasic AJ, Chasen NM, Dykes EJ, Vella SA, Asady B, Starai VJ, Moreno SNJ. 2019. The Toxoplasma Vacuolar H(+)-ATPase Regulates Intracellular pH and Impacts the Maturation of Essential Secretory Proteins. Cell Rep 27:2132-2146 e7.
62. Roos DS, Donald RG, Morrissette NS, Moulton AL. 1994. Molecular tools for genetic dissection of the protozoan parasite Toxoplasma gondii. Methods Cell Biol 45:27-63.
63. Bertolini MS, Chiurillo MA, Lander N, Vercesi AE, Docampo R. 2019. MICU1 and MICU2 Play an Essential Role in Mitochondrial Ca(2+) Uptake, Growth, and Infectivity of the Human Pathogen Trypanosoma cruzi. mBio 10.

64. Ling Y, Sahota G, Odeh S, Chan JM, Araujo FG, Moreno SN, Oldfield E. 2005. Bisphosphonate inhibitors of Toxoplasma gondi growth: in vitro, QSAR, and in vivo investigations. J Med Chem 48:3130-40.
65. van Dooren GG, Tomova C, Agrawal S, Humbel BM, Striepen B. 2008. Toxoplasma gondii Tic20 is essential for apicoplast protein import. Proc Natl Acad Sci U S A 105:13574-9.
66. Recher M, Barboza AP, Li ZH, Galizzi M, Ferrer-Casal M, Szajnman SH, Docampo R, Moreno SN, Rodriguez JB. 2013. Design, synthesis and biological evaluation of sulfur-containing 1,1-bisphosphonic acids as antiparasitic agents. Eur J Med Chem 60:431-40.
67. Canavaci AM, Bustamante JM, Padilla AM, Perez Brandan CM, Simpson LJ, Xu D, Boehlke CL, Tarleton RL. 2010. In vitro and in vivo high-throughput assays for the testing of anti-Trypanosoma cruzi compounds. PLoS Negl Trop Dis 4:e740.

Tables

Table 1: Enzymatic Characterization of recombinant TgCoq1. Allylic substrate specificity of TgCoq1. The concentration of the allylic substrates (GPP, FPP, GGPP and IPP) was varied, and the counter substrate concentration was kept at a saturating level. The nonlinear regression analysis (Sigma plot 10.0) was used to calculate the Kinetic parameters. Values shown are means ± SD of two independent experiments performed in duplicate. The values of k_{cat}/K_m show that the enzyme is more efficient with FPP as the allylic substrate.

Substrate	Counter Substrate	K_m (μMolar)	V_{max} (nmoles/min/mg)	K_{cat} (min^{-1})	K_{cat}/K_m (min^{-1} x $Mole^{-1}$)
GPP	IPP (100μM)	0.88 ± 0.60	6.16 ± 0.45	0.012 ± 0.001	13.63
FPP	IPP (100μM)	12.37 ± 1.83	226.13 ± 7.56	0.452 ± 0.015	36.54
GGPP	IPP (100μM)	14.05 ± 1.43	82.98 ± 2.51	0.165 ± 0.005	11.74
IPP	GPP (150μM)	145.48 ± 1.18	28.30 ± 0.16	0.057 ± 0.001	0.39
IPP	FPP (100μM)	139.11 ± 17.68	560.54 ± 46.09	1.12 ± 0.092	8.05
IPP	GGPP (50μM)	141.89 ± 35.75	372.92 ± 65.53	0.745 ± 0.131	5.25

Table 2. Inhibition of growth and the recombinant enzymes TgFPPS and TgCoq1 by selected bisphosphonates. * These compounds showed inhibition of at least 50% at 10 µM

Compounds	Structures	Growth IC_{50} (µM)*	TgFPPS IC_{50} (µM)	TgCoq1 IC_{50} (µM)
BPH-1218	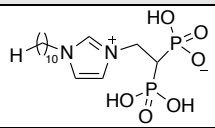	0.32 ± 0.04	0.173 ± 0.042	0.036 ± 0.007
BPH-1236	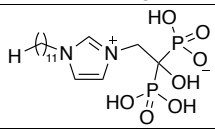	0.59 ± 0.22	0.503 ± 0.053	0.041 ± 0.002
BPH-1238	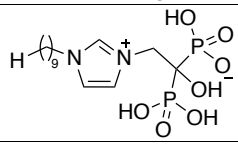	0.68 ± 0.30	0.046 ± 0.012	0.036 ± 0.004
BPH-1328	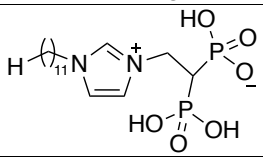	0.68 ± 0.35	0.096 ± 0.059	0.072 ± 0.005
BPH-703	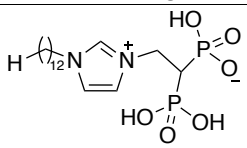	0.81 ± 0.18	0.190 ± 0.105	0.111 ± 0.028
BPH-252	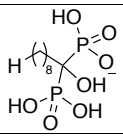	0.85 ± 0.14	0.132 ± 0.054	2.129 ± 0.517
BPH-1327	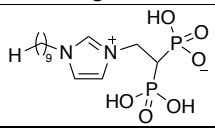	1.04 ± 0.30	0.008 ± 0.000	0.090 ± 0.007
BPH-1219	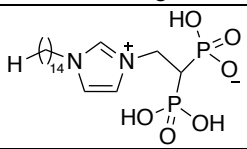	1.14 ± 0.36	0.689 ± 0.036	0.657 ± 0.001
BPH-1222	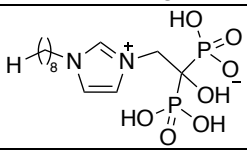	1.55 ± 0.32	0.184 ± 0.014	0.155 ± 0.012
BPH-1325	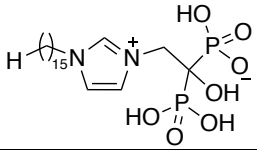	1.65 ± 0.89	0.702 ± 0.057	1.693 ± 0.465
BPH-1338	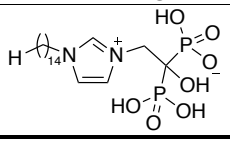	1.81 ± 0.53	0.854 ± 0.326	1.540 ± 0.249

Table 3: IC_{50} of BPH-1218 on TgCoq1-OE strain is significantly higher than parental strain while IC_{50} of drugs atovaquone and SQ-109 was not affected by TgCoq1 overexpression. Enzymatic activity shows that TgCoq1 is a more specific target than TgFPPS for BPH-1218.

Drug	Structure	EC_{50} (μM) (parental strain)	EC_{50} (μM) TgCoq1-OE strain
BPH-1218		0.92 ± 0.09	2.86 ± 0.75
Atovaquone		0.033 ± 0.013	0.044 ± 0.011
SQ109		1.73 ± 0.38	1.80 ± 0.47

Table 4: EC_{50} for *T. gondii* RH growth inhibition measured with and without the addition of ubiquinone Q_6 to the culture. Values are means ± s.d. of n = 3.

Compound	Structure	EC_{50} (μM)	EC_{50} (μM) + UQ_6
BPH-1218		0.32 ± 0.04	8.27 ± 6.14
BPH-1236		0.99 ± 0.37	2.33 ± 0.83
BPH-1217		7.10 ± 2.02	11.07 ± 1.66
BPH-1219		11.56 ± 0.98	7.65 ± 3.54
JAG-21		0.049 ± 0.02	0.07 ± 0.001

FIGURES

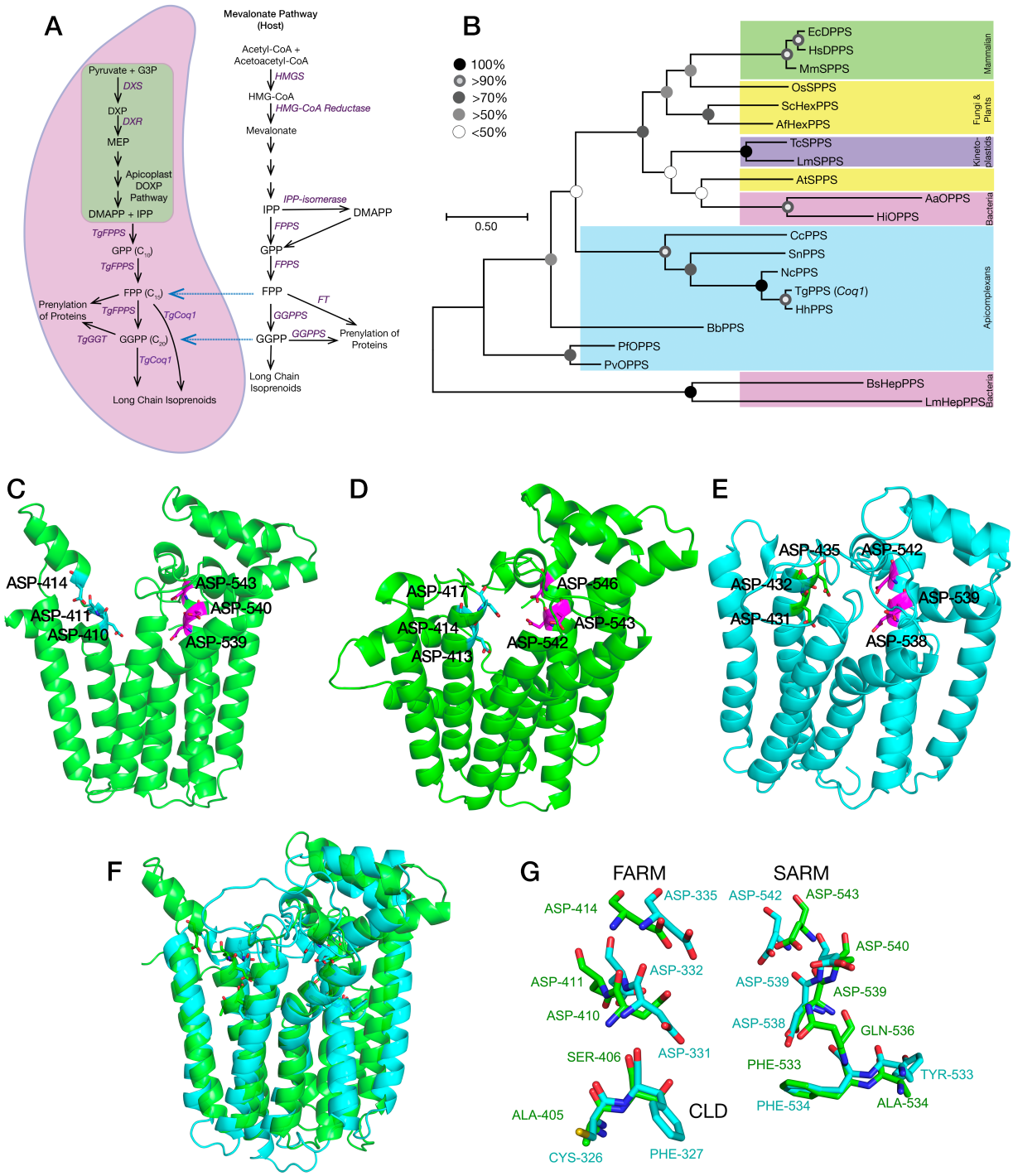
A
Mevalonate Pathway (Host)
Pyruvate + G3P
DXS
DXP
DXR
MEP
Apicoplast DOXP Pathway
DMAPP + IPP
TgFPPS
GPP (C10)
FPP (C15)
Prenylation of Proteins
TgGGT
GGPP (C20)
TgCoq1
Long Chain Isoprenoids
Acetyl-CoA + Acetoacetyl-CoA
HMGS
HMG-CoA
HMG-CoA Reductase
Mevalonate
IPP
IPP-isomerase
DMAPP
FPPS
GPP
FPP
FT
GGPPS
GGPP
Prenylation of Proteins
Long Chain Isoprenoids
B
100%
>90%
>70%
>50%
<50%
0.50
EcDPPS
HsDPPS
MmSPPS
Mammalian
OsSPPS
ScHexPPS
AfHexPPS
Fungi & Plants
TcSPPS
LmSPPS
Kinetoplastids
AtSPPS
AaOPPS
HiOPPS
Bacteria
CcPPS
SnPPS
NcPPS
TgPPS (Coq1)
HhPPS
BbPPS
PfOPPS
PvOPPS
Apicomplexans
BsHepPPS
LmHepPPS
Bacteria
C
ASP-414
ASP-411
ASP-410
ASP-543
ASP-540
ASP-539
D
ASP-417
ASP-414
ASP-413
ASP-546
ASP-543
ASP-542
E
ASP-435
ASP-542
ASP-432
ASP-539
ASP-431
ASP-538
F
G
FARM
ASP-414
ASP-335
ASP-411
ASP-332
ASP-410
ASP-331
SER-406
ALA-405
CLD
CYS-326
PHE-327
SARM
ASP-542
ASP-543
ASP-540
ASP-539
ASP-539
ASP-538
GLN-536
PHE-533
TYR-533
PHE-534
ALA-534

Figure 1. Phylogenetic placing and predicted structure of the *Toxoplasma* polyprenyl synthase (TgCoq1) and its predicted role in the isoprenoid pathway. A, the isoprenoid (DOXP/MEP) pathway of *T. gondii* compared to the host Mevalonate (MVA) pathway. G3P, glyceraldehyde 3-phosphate; DXP, deoxyxylulose 5-phosphate; DXS, DXP synthase; DXR, deoxyxylulose 5-phosphate reductoisomerase; MEP, methyl-D-erythritol phosphate; DMAPP, dimethyl ally diphosphate; IPP, isopentenyl diphosphate; GPP, geranyl diphosphate; FPP, farnesyl diphosphate; FPPS, farnesyl diphosphate synthase; GGPP, geranylgeranyl diphosphate; GGT, geranylgeranyl transferase; HMGS, 3-hydroxy-3-methylglutaryl-CoA synthase; FT, farnesyl transferase; GGPPS, geranylgeranyl diphosphate synthase. The *blue arrows* represent the intermediate metabolites that can be salvaged from the host. **B**, Phylogenetic analysis of enzymes of the isoprenoid pathway from various organisms. The sequences used are listed in supplemental Table S1. The enzymes are HexPPS, hexaprenyl pyrophosphate synthase; HepPPS, heptaprenyl pyrophosphate synthase; OPPS, octaprenyl pyrophosphate synthase; SPPS, solanesyl pyrophosphate synthase; DPPS, decaprenyl pyrophosphate synthase and PPS, polyprenyl synthase. The analysis shows substitutions per site for *Arabidopsis thaliana* SPPS (NP_17792.2), *Oryza sativa* SPPS (Q653T6.1), *Saccharomyces cerevisiae* HexPPS (P18900.1), *Trypanosoma cruzi* SPPS (EAN82722.1), *Leishmania major* SPPS (XP_001682016.1), *Plasmodium falciparum* OPPS (XP_001349541.1), *Plasmodium vivax* OPPS (VUZ93874.1), *Toxoplasma gondii* polyprenyl synthase (TgCoq1) trimmed (XP_018636584.1), *Neospora caninum* PPS (XP_003883948.1), *Hammondia hammondi* PPS trimmed (HHA_269430), *Cyclospora cayetanensis* PPS (LOC34620908), *Sarcocystis neurona* PPS trimmed (SN3_03700020), *Babesia bovis* PPS (EDO07087.1), *Bacillus subtilis* HPPPS (ARW31988.1), *Listeria monocytogenes* HepPPS (QGK56962.1), *Aquifex aeolicus* OPPS (NP_213606.1), *Haemophilus influenzae* HepPPS (CBY85984.1), *Aspergillus fumigatus* DPPS (EDP53123.1), *Mus musculus* SPPS (BAE48219.1), *Equus caballus* DPPS (XP023487828.1), and *Homo sapiens* DPPS (BAE48216.1). **C,** Phyre2 prediction based on the full TgCoq1sequence: only the catalytic domain is predicted, and it is as found in other *trans*- head-to-head prenylsynthases. The catalytic Asps in the two DDxxD motifs are indicated. **D**, Phyre2 prediction based on the full HhFPPS sequence. **E**, Phyre2 prediction based on the full TgFPPS sequence. **F**, Superposition of TgCoq1 (green) and TgFPPS (cyan) predicted structures. **G**, Zoomed-in version of F.

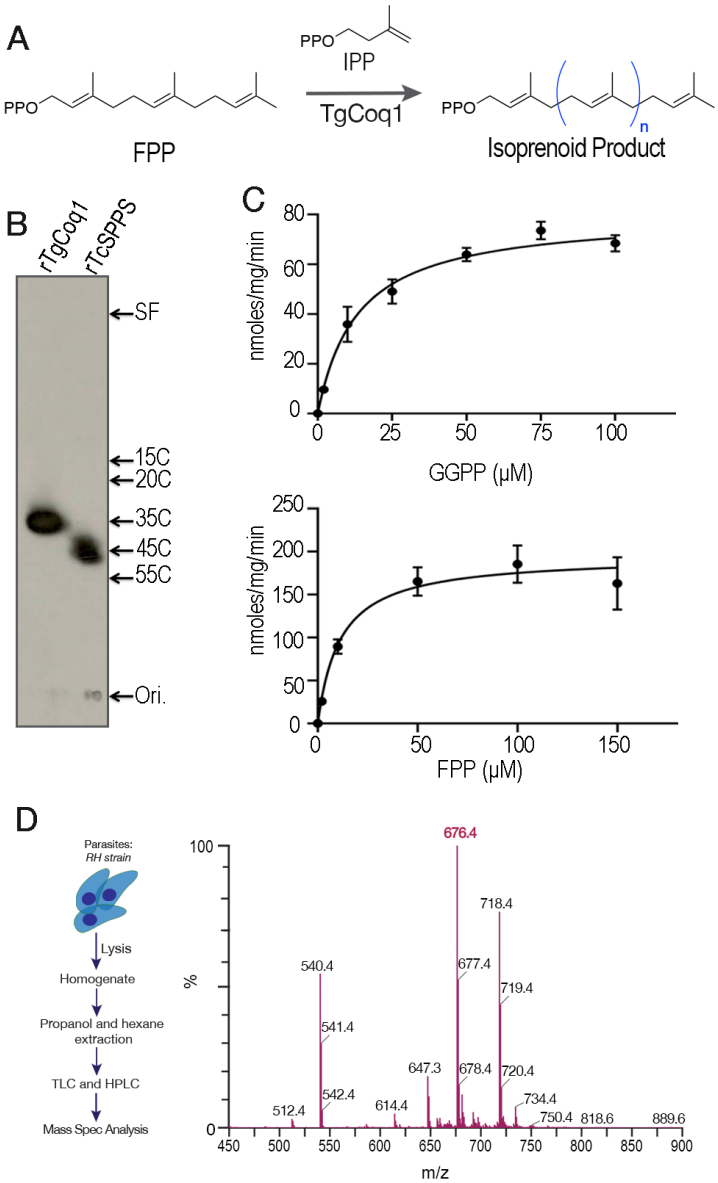

Figure 2. TgCoq1 catalyzes the synthesis of long chain isoprenoids from FPP. **A**, Scheme of the reaction catalyzed by Coq1. **B**, Analysis of the products formed by rTgCoq1 by thin-layer chromatography. The size of the product made by rTgCoq1 has 35 carbons (heptaprenyl). The reaction catalyzed by the *T. cruzi* solanesyl diphosphate synthase was run in parallel (rTcSPPS). Commercial standards of various chain lengths were run in the same system. SF is the solvent front and Ori. is the loading level of the samples. **C**, Specific activity assays of recombinant TgCoq1. Graphical data supporting the calculations of K_m and V_{max} for TgCoq1 are presented in Table 1. **D**, Mass spec analysis of *T. gondii* extracts obtained by 1-propanol followed by hexane extraction (see methods). Extracts were first purified by TLC, followed by HPLC prior to mass spec.

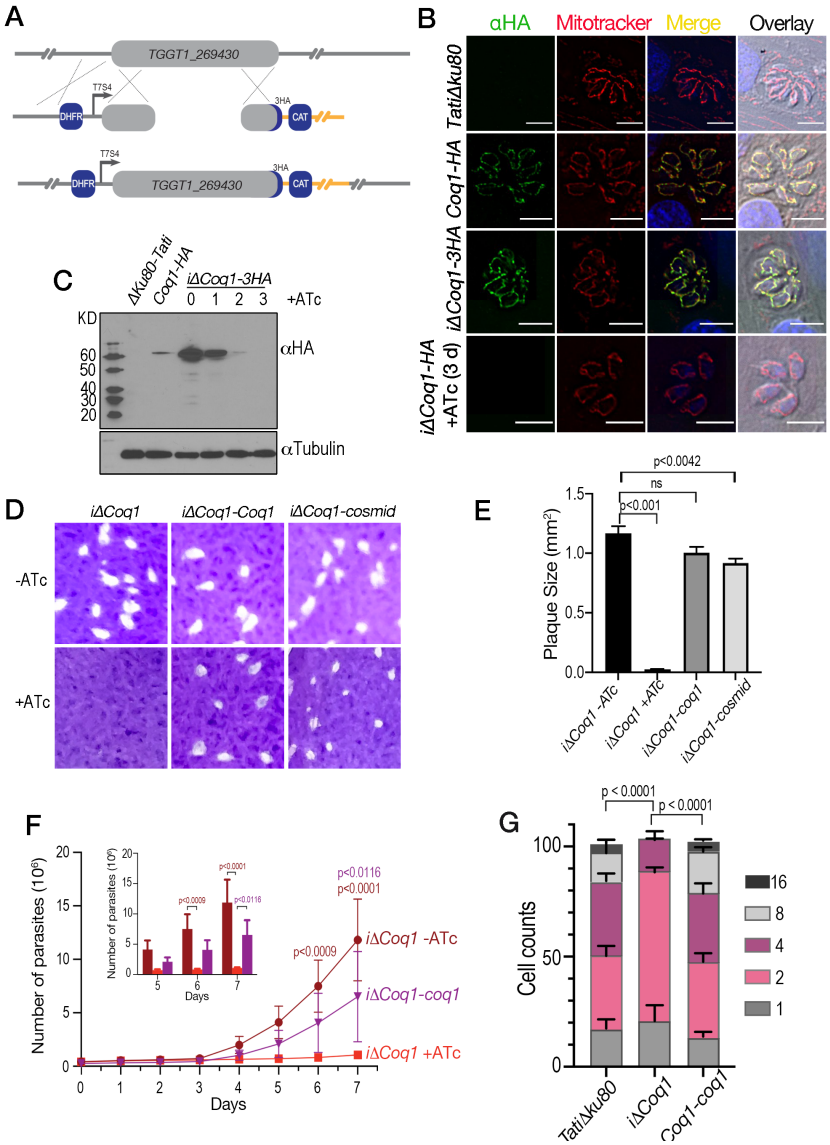

Figure 3. TgCoq1 is essential for *T. gondii* growth and localizes to the mitochondria. A, Strategy used to tag the *TgCoq1* gene locus with 3xHA and promoter replacement strategy for generation of the *iΔCoq1-3xHA* mutant. The endogenous TgCoq1 promoter is replaced with a Tet7Sag4 (T7S4) tetracycline inducible promoter. Expression of the dihydrofolate reductase (DHFR) confers pyrimethamine resistance and was used as a selectable marker. **B**, Immunofluorescence showing TgCoq1 localization to the mitochondria. Mitotracker was used to stain the mitochondria, and anti-HA antibody to localize TgCoq1. The TgCoq1 signal in the *iΔCoq1-3xHA* mutant at 0 and after 3 days of growth with 0.5 µg/ml ATc. **D,** Plaque assay showing that the *iΔCoq1* mutant was unable to form plaques when grown with ATc. Parasites were pre-incubated with ATc for 3 days prior to the experiment. Growth was restored by complementation with *TgCoq1* cDNA or with a cosmid containing the full *TgCoq1* genomic locus. **E**, Plaque size quantification from three biological experiments. **F**, Growth assay of RFP expressing cells highlighting the growth defect of the *iΔCoq1* mutant and its rescue by complementation with TgCoq1 cDNA. **G**, Parasite replication assay showing the parasites/vacuole for each of the strains. Analysis was performed from three independent biological experiments, each one in triplicate. Statistical analysis for E, F and G was done using Student's t-test.

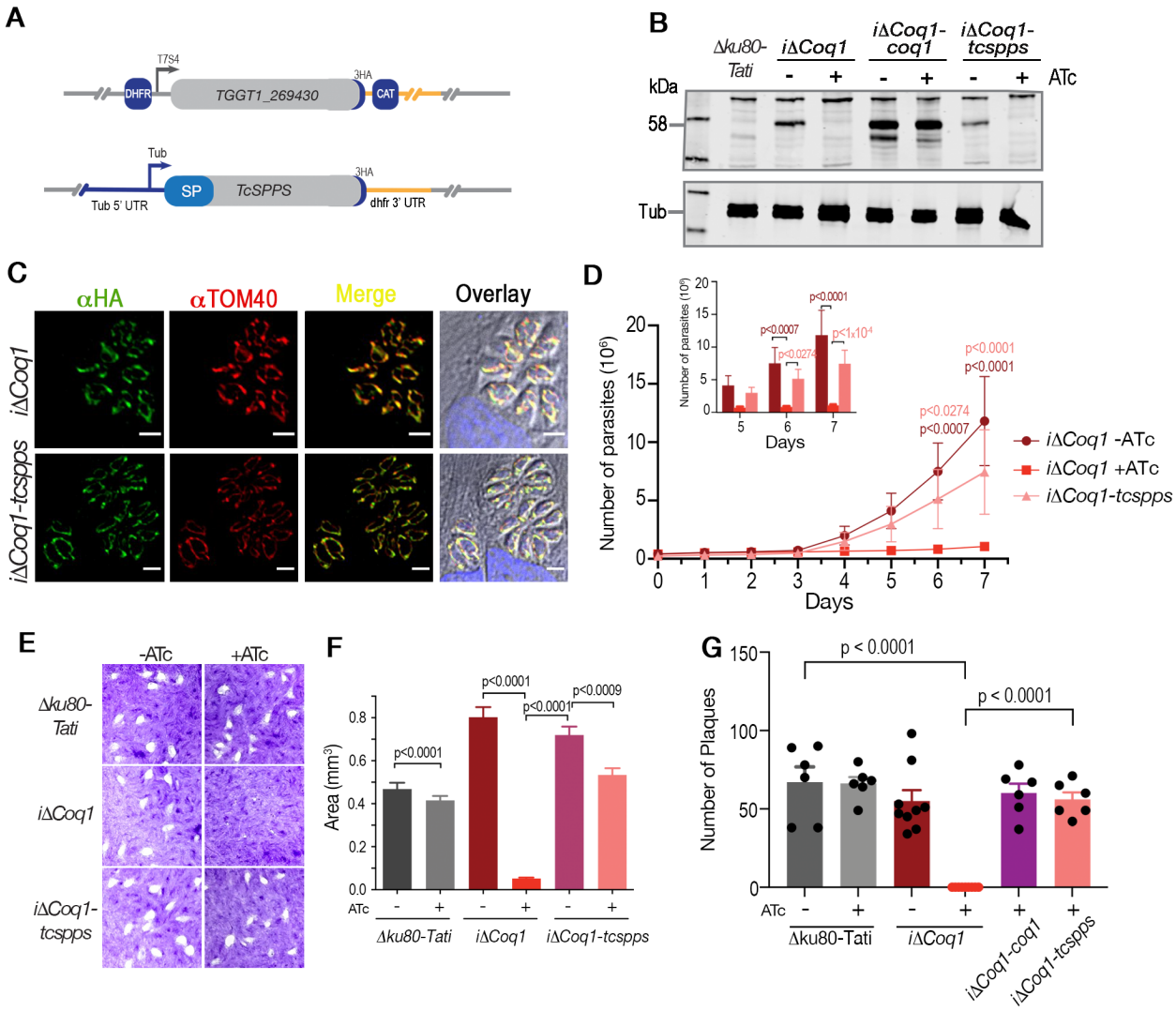

Figure 4. A different isoprenoid tail can replace the one synthesized by TgCoq1. A, Model depicting the complementation of the promoter insertion cells line (*iΔCoq1*) with a *T. cruzi* SPPS in the pCTH3 plasmid backbone. **B**, Western blots with the polyclonal antibody against TgCoq1 (αTgCoq1) showing that the signal of TgCoq1 disappears in cells cultured with ATc. Tubulin was used for loading control. **C**, IFAs with αHA showing the localization of TcSPPS to the mitochondria of intracellular parasites. *iΔCoq1-spps* cells were continuously cultured with ATc and as shown in Fig. 3C there is no expression of the parental Coq1. **D**, Growth assay of RFP expressing cell lines showing that the growth defect of the *iΔCoq1* mutant is restored by complementation with the *T. cruzi* SPPS. **E**, Plaque assay showing that the *iΔCoq1* mutant was unable to form plaques when cultured with ATc, and growth was restored by expression of TcSPPS. **F,** Quantification of the area of fifteen plaques from each of 3 assays like the one shown in E. **G,** Plaquing efficiency assay in which plaque numbers were quantified from 3 biological replicates. The analyses presented in D, F and G were from three independent biological experiments using Student's t-test.

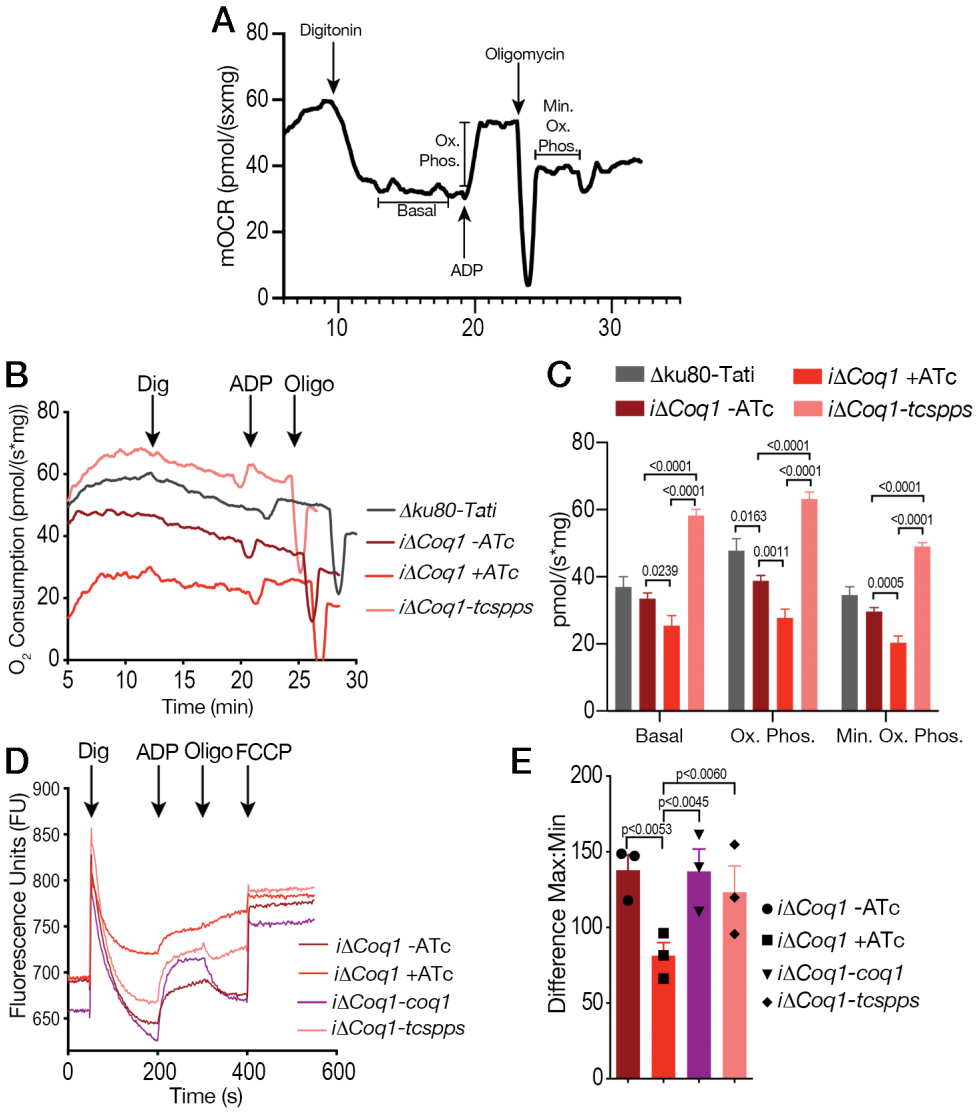

Figure 5. TgCoq1 is essential for mitochondrial function. A, Oxygen consumption rate (OCR) of RH*Δku80* parasites showing the computed parameters of each condition. **B,** OCR experiments measuring oxygen consumption of the *iΔCoq1* mutant showing a reduction in oxygen consumption after 3 days of incubation with 0.5 µg/ml ATc that is restored in the *T. cruzi* SPPS complemented cell lines also grown with 0.5 µg/ml ATc for 3 days. **C,** Quantification of peaks from the OCR experiments showing significant differences of the parental cell lines, *iΔCoq1*, and the *iΔCoq1-tcspps* complemented ones. **D,** Mitochondrial membrane potential (ΔΨm) of the *iΔCoq1* mutant without ATc and with 0.5 µg/ml ATc for 3 days. Defect in ΔΨm of the *iΔCoq1* mutant was detected after 3 days with ATc. Complementation with the TcSPPS gene restored the defect. Digitonin (Dig) was added at 50 sec, Adenosine diphosphate (ADP) was added at 200 sec, Oligomycin (Oligo) was added at 300 sec, and Carbonyl cyanide-4-(trifluoromethoxy) phenylhydrazone (FCCP) was added at 400 sec. **E,** Quantification of the mitochondrial membrane potential, the difference was calculated by subtracting the minimum after digitonin from the maximum peak after addition of FCCP. The dots represent each of 3 biological replicates which are the averages from 3 technical replicates. The analyses were done from three independent biological experiments using Student's t-test.

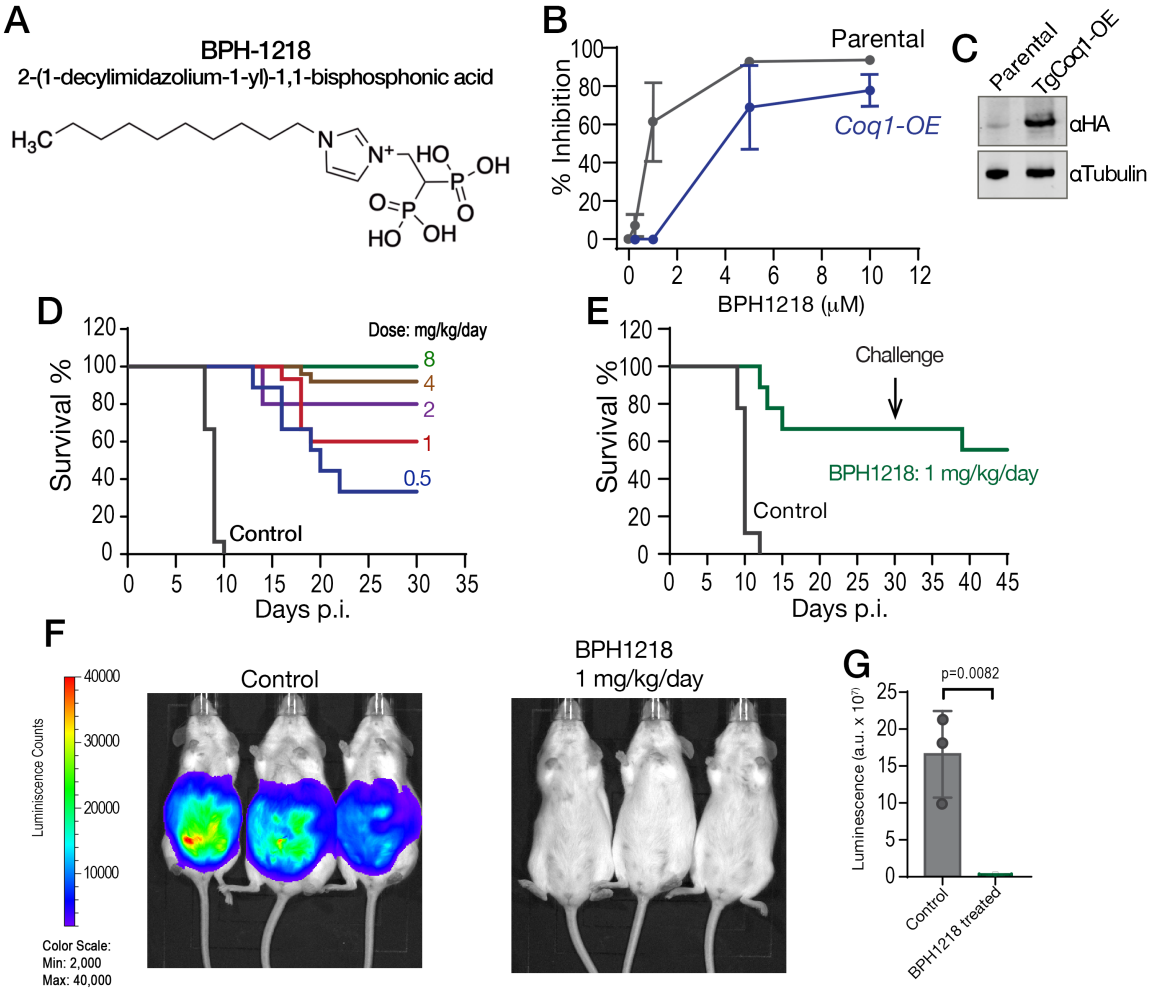

Figure 6. Targeting TgCoq1 with a lipophilic bisphosphonate. **A,** Structure of BPH-1218. **B,** % inhibition by the drug BPH-1218 of the parental and the TgCoq1 over-expressing mutant (Coq1-OE) showing that the Coq1-OE is more resistant to BPH-1218. **C,** Western blot analysis showing the increase in expression of the HA tagged TgCoq1 in the overexpressing cell line. **D,** BPH-1218 protects against a lethal *in vivo* infection in mice. The indicated doses (mg/kg/day) of BPH-1218 were inoculated for 10 days after mice were infected with a lethal dose of RH parasites. ED_{50} = 0.69 mg/kg/day (data summarized from three independent experiments). **E,** Challenge with 100 RH parasites of living mice on day 30 after treatment for 10 days with 1 mg/kg/day BPH-1218. **F,** Infection of mice with a luciferase-expressing strain of RH parasites shows BPH treatment of mice clears the infection. **G,** Quantification of luciferase expression.

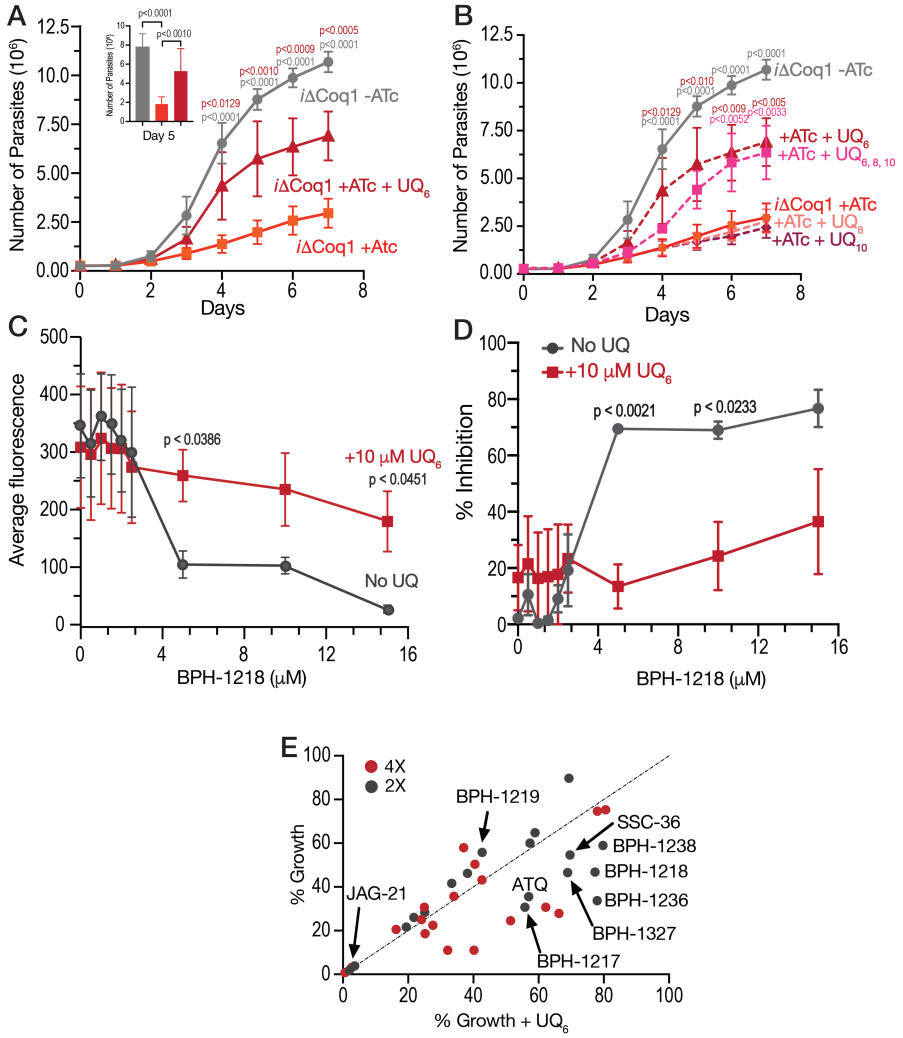

Figure 7. **Ubiquinone 6 rescues the growth defect of the *iΔCoq1* mutant and the growth inhibition by BPH-1218**. **A,** Growth of the *iΔCoq1* mutant with ATc is rescued by addition of 10 μM UQ_6. **B,** Growth of the *iΔCoq1* with ATc supplemented with 5 μM Ubiquinone 8 (UQ8) and Ubiquinone 10 (UQ10) shows no rescue of the growth defect. Only UQ_6 shows rescue at 5 μM. **C**, Inhibition by BPH-1218 is rescued by addition of 10 μM UQ_6 to the culture. **D**, % inhibition by BPH-1218 with and without UQ_6. **E,** UQ_6 rescue screen of 18 compounds at 2X and 4X their known EC_{50}. Drugs that are rescued by UQ_6 are shifted to the right from the dotted line. The dots are averages from 3 biological replicates. The compounds not labeled in the graph are BPH-1327, BPH-1238, Atovaquone, Pyrimethamine, BPH-754, Risedronate, SSC-36, CE-22, MNC-98, CE-29, MNCA181, CE-109, and CE-91. Structures shown in Table S5.